The Impact of the North Atlantic Oscillation on Climate through Its Influence on the Atlantic Meridional Overturning Circulation

THOMAS L. DELWORTH AND FANRONG ZENG

NOAA/Geophysical Fluid Dynamics Laboratory, Princeton, New Jersey

(Manuscript received 4 June 2015, in final form 6 November 2015)

ABSTRACT

The impact of the North Atlantic Oscillation (NAO) on the Atlantic meridional overturning circulation (AMOC) and large-scale climate is assessed using simulations with three different climate models. Perturbation experiments are conducted in which a pattern of anomalous heat flux corresponding to the NAO is added to the model ocean. Differences between the perturbation experiments and a control illustrate how the model ocean and climate system respond to the NAO. A positive phase of the NAO strengthens the AMOC by extracting heat from the subpolar gyre, thereby increasing deep-water formation, horizontal density gradients, and the AMOC. The flux forcings have the spatial structure of the observed NAO, but the amplitude of the forcing varies in time with distinct periods varying from 2 to 100 yr. The response of the AMOC to NAO variations is small at short time scales but increases up to the dominant time scale of internal AMOC variability (20–30 yr for the models used). The amplitude of the AMOC response, as well as associated oceanic heat transport, is approximately constant as the time scale of the forcing is increased further. In contrast, the response of other properties, such as hemispheric temperature or Arctic sea ice, continues to increase as the time scale of the forcing becomes progressively longer. The larger response is associated with the time integral of the anomalous oceanic heat transport at longer time scales, combined with an increased impact of radiative feedback processes. It is shown that NAO fluctuations, similar in amplitude to those observed over the last century, can modulate hemispheric temperature by several tenths of a degree.

1. Introduction

One of the central challenges in climate research is to increase our ability to quantify the role of natural variability and anthropogenic forcing in observed climate change (Bindoff et al. 2013). We seek to quantify what fraction of observed changes in the climate system has come from anthropogenic and natural radiative forcing changes and what fraction from internal variability. A key goal is therefore to improve our understanding of the mechanisms of natural climate variability, particularly on decadal and longer time scales.

Two important phenomena associated with climate variability are the North Atlantic Oscillation (NAO) and the Atlantic meridional overturning circulation (AMOC). These two phenomena have been associated with a wide range of climate variations across the Northern Hemisphere on a variety of time scales (Hurrell 1995, 1996; Hurrell and Deser 2009; Trigo et al. 2002). The NAO is primarily an atmospheric phenomenon, characterized by subseasonal to multidecadal variations in storm tracks over the North Atlantic sector (Gerber and Vallis 2009). Extensive previous work has shown that atmospheric circulation changes associated with the NAO drive an array of climate variations over North America and Europe (Cullen et al. 2002; Trigo et al. 2002; Scaife et al. 2008). These variations are clearly linked with changes in large-scale atmospheric circulation and corresponding precipitation and temperature anomalies.

The AMOC consists of a northward flow of relatively warm, salty water in the upper layers of the Atlantic and a southward return flow at depth (Kuhlbrodt et al. 2007). The associated release of heat to the atmosphere at higher latitudes of the North Atlantic has a major impact on climate and climate variability. A rich history of modeling studies (Delworth et al. 1993; Visbeck et al. 1998; Zhu and Jungclaus 2008; Park and Latif 2008; Biastoch et al. 2008; Vellinga and Wu 2004; Frankcombe

Corresponding author address: Thomas L. Delworth, NOAA/Geophysical Fluid Dynamics Laboratory, 201 Forrestal Rd., Princeton University Forrestal Campus, Plainsboro, NJ 08540.
E-mail: tom.delworth@noaa.gov

DOI: 10.1175/JCLI-D-15-0396.1

et al. 2010; Danabasoglu et al. 2012; Medhaug et al. 2012; Menary et al. 2012; Kwon and Frankignoul 2012; Tulloch and Marshall 2012; Yeager and Danabasoglu 2012) has shown that the AMOC can have substantial variability on decadal-to-centennial time scales. In addition, the AMOC can have a significant influence on climate on many time scales (Delworth and Mann 2000; Knight et al. 2005; Frierson et al. 2013; Frankignoul et al. 2013). Variations in the AMOC are viewed as an important driver of the observed Atlantic multidecadal oscillation, which in turn influences hemispheric climate (Zhang et al. 2007; Chylek et al. 2009; Sutton and Dong 2012; Li et al. 2013; Steinman et al. 2015).

Previous modeling work has shown a clear connection between the NAO and the AMOC (Visbeck et al. 1998; Delworth and Greatbatch 2000; Delworth and Dixon 2000; Eden and Jung 2001). Variations in the NAO have been hypothesized to play a role in AMOC variations by modifying air–sea fluxes of heat, water, and momentum. These flux variations alter vertical and horizontal density gradients in the subpolar North Atlantic, thereby inducing changes to deep-water formation and the AMOC.

In this study we examine the connections between NAO variations, the AMOC, and larger-scale climate through the use of large suites of climate model simulations. We design experiments to specifically examine how variations in surface fluxes associated with the NAO can induce AMOC variations and how these AMOC variations in turn influence large-scale climate. We adopt an idealized modeling framework that allows us to examine how different time scales of NAO variations influence the AMOC and the larger climate system. Our methodology involves the use of simulations in which we artificially impose NAO-like fluxes on the model ocean and assess the response of the model ocean and larger-scale climate to these NAO-like variations. Recent work has suggested that multidecadal NAO variations can be used as a predictor of Northern Hemispheric temperature (Li et al. 2013), and in this study we conduct simulations that provide a physically based underpinning for that connection.

2. Models and experimental design

a. Models

We use three versions of GFDL climate models in this study. The first is the GFDL CM2.1 model (Delworth et al. 2006). This is a fully coupled ocean–atmosphere model, with land and atmospheric resolution of approximately 200 km in the horizontal and 24 vertical levels in the atmosphere. The ocean component has horizontal resolution of approximately 100 km, with finer resolution in the tropics, and 50 levels in the vertical. This model has been used in a wide variety of studies of climate variability, predictability, and change, and extensive model output from past studies is available online (http://nomads.gfdl.noaa.gov/CM2.X/ and http://nomads.gfdl.noaa.gov:8080/DataPortal/cmip5.jsp). The second model used is the Forecast-Oriented Low Ocean Resolution (FLOR) version of GFDL CM2.5 (CM2.5_FLOR, hereinafter referred to as FLOR; Vecchi et al. 2014). This model uses atmospheric physics that are very similar to CM2.1 but has a higher spatial resolution in the atmosphere as well as a much improved land model (LM3; Milly et al. 2014). The horizontal resolution of the atmosphere and land model is approximately 50 km (versus 200 km in CM2.1). The number of vertical levels in the atmosphere has increased from 24 in CM2.1 to 32 in FLOR. The ocean component of FLOR is similar to that in CM2.1. The third model used is GFDL CM3 (Donner et al. 2011; Griffies et al. 2011). This has a similar horizontal spatial resolution in the atmosphere as CM2.1 but has substantially increased vertical resolution (48 layers), as well as including representations of the indirect effect of aerosols and interactive chemistry. As in the other two models, the horizontal resolution of the ocean component is approximately 1°.

Millennial-scale control simulations have been conducted with each model using radiative forcing conditions representative of preindustrial conditions, corresponding to approximately calendar year 1860.

b. Experimental design

We wish to assess how the model ocean responds to idealized variations in the NAO and then alters the rest of the climate system. In particular, we wish to study the response of the AMOC to idealized NAO variations and how those changes in the AMOC impact the rest of the climate system. We do this by designing simulations in which the model ocean "feels" an arbitrary phase of the NAO. In these simulations we intervene in the model whenever the model atmosphere and ocean exchange fluxes (described in detail below). As a result, the model ocean reacts to arbitrarily imposed NAO flux anomalies. By comparing the differences between ensembles of simulations with and without this artificial NAO forcing, we can assess how the AMOC and model climate system respond to the NAO.

We first create patterns of flux forcing that correspond to the NAO. We start with time series of monthly mean surface fluxes (heat, water, and momentum) from the ECMWF interim reanalysis (ERA-Interim; Dee et al. 2011) as well as the time series of the observed

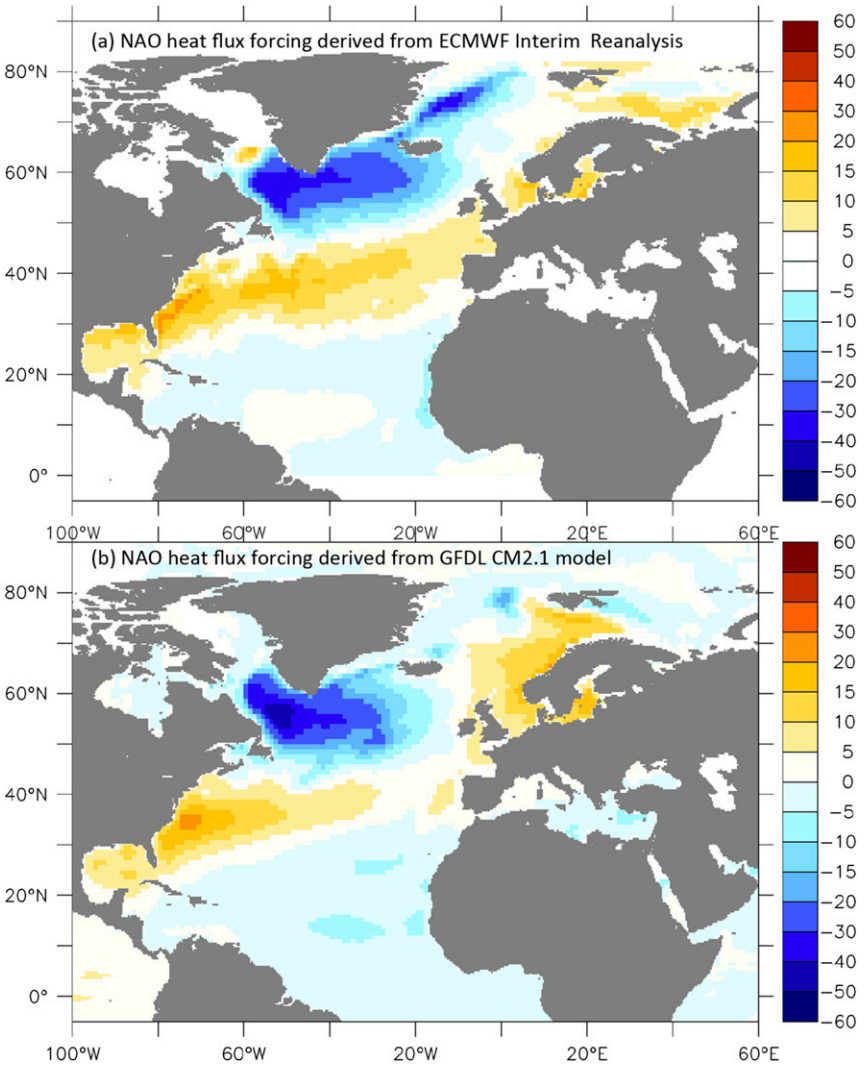

FIG. 1. Spatial pattern of the heat flux anomalies (W m^{-2}) used as anomalous flux forcings in the model experiments. Negative values mean a flux of heat from the ocean to the atmosphere. (a) Fluxes derived from ERA-Interim—the mean fluxes over December–March that correspond to a one-standard-deviation anomaly of the NAO. (b) Fluxes from a long control simulation of CM2.1, corresponding to a one-standard-deviation anomaly of the NAO.

NAO using a station-based index (downloaded from the NCAR–UCAR climate data guide at https://climatedataguide.ucar.edu/climate-data/hurrell-north-atlantic-oscillation-nao-index-station-based; the NAO index is defined as the difference between a normalized time series of SLP from Lisbon, Portugal, and a normalized time series of SLP from Reykjavik, Iceland, using seasonal means over December–March). We then create 4-month averages from the ERA-Interim data over the December–March period. We compute the linear regression coefficients at each grid point between the time series of the reanalysis fluxes (heat, water, and momentum) and the NAO. In Fig. 1 we show the regression map for surface heat flux anomalies, indicating the pattern of surface heat flux change accompanying an increase of one standard deviation in the NAO. For use as described below, we scale the ECWMF-derived regression coefficients for the flux fields by one standard deviation of the NAO index time series. We use the flux forcing only over the Atlantic from the equator to 82°N, including the Barents Sea and Nordic seas. We adjust the fluxes so that their areal integral is zero. In this manner, the imposed heat fluxes do not provide a net heating or cooling to the system.

The coupled models normally compute air–sea fluxes of heat, water, and momentum that depend on the gradients in these quantities across the air–sea interface. In our perturbation experiments this process continues, but

after these fluxes are calculated we add an additional flux component to the model ocean. The model ocean therefore receives the fluxes that are computed based on air–sea gradients plus an extra flux that corresponds to a specified phase of the NAO. We have conducted simulations with additions of heat, water, and momentum fluxes. However, sensitivity studies have shown that for this model the heat flux anomalies dominate the response, and so we show results from simulations that are driven only by adding anomalous heat fluxes.

We create time series of NAO-derived fluxes that have idealized variations in time. In one set of experiments, referred to as ''switch on,'' we suddenly turn on the extra NAO flux forcing at an arbitrary point in the control simulation and leave these extra fluxes on with a constant amplitude corresponding to one standard deviation of the observed NAO time series. These experiments elucidate the adjustment process of the climate system in response to an instantaneous imposition of the extra NAO fluxes. We also conduct suites of experiments in which we add NAO fluxes whose amplitude is modulated sinusoidally in time with a single time scale. We conduct separate ensembles of simulations in which the NAO is modulated with periods of 2, 5, 10, 20, 50, and 100 yr. The amplitude of the extra NAO forcing time series corresponds to one standard deviation of the observed NAO time series. We note that these are highly idealized sequences of NAO forcing that allow us to systematically examine the response of the ocean to various time scales of NAO forcing and are not meant to represent the observed NAO time series. In all experiments the NAO forcing is applied only in the months of December through March, with a constant value for that period and a linear taper at the start and end of this period. This is the primary season of oceanic convection and deep-water formation at higher latitudes of the North Atlantic.

Analyses of the spectral characteristics of the observed NAO suggest that it is fairly similar to white noise, with variance on all time scales but with some suggestion of spectral peaks around 2 and 7–10 yr (Gámiz-Fortis 2002), as well as multidecadal variability (Li et al. 2013). However, the shortness of the instrumental record means that the robustness of the peaks is questionable, especially at longer time scales (Wunsch 1999). Our simulations are designed to probe the response of the climate system to idealized NAO forcing across a wide range of time scales, consistent with a white noise process that contains variance at all time scales.

To more clearly identify the response to the NAO, all experiments are conducted as ensembles. For the CM2.1 simulations we use 10-member ensembles. The 10 members start from 10 different points in a long control simulation, with each of the points separated by 40 years. This separation is longer than the dominant time scale of AMOC internal variability in the model in order to reduce the likelihood of aliasing effects. For analysis we examine the ensemble mean of the perturbed experiments and contrast that with the ensemble mean of the corresponding sections of the control simulation. For FLOR and CM3 we use five-member ensembles, primarily because of the greater computational expense associated with the higher-resolution models.

In our experimental design we can impose NAO-related fluxes of heat, water, or momentum. Preliminary simulations (not shown) have indicated that variations in heat flux have a dominant impact on the AMOC in these models for the decadal-scale variability being examined. Therefore, in subsequent experiments we impose only NAO-related changes in heat flux. However, it is possible that the ocean model used here does not respond as energetically to momentum fluxes as it should, possibly as a consequence of its relatively coarse resolution. Additional studies with higher-resolution models that produce more energetic flow should reassess this issue. This is particularly relevant in light of the impact of observed wind stress anomalies for AMOC variability on interannual time scales (Roberts et al. 2013).

We have conducted simulations using NAO-related surface fluxes both as defined from ERA-Interim and as evaluated from a long control integration of CM2.1 (pattern shown in Fig. 1b). Since the results were fairly similar when using either set of fluxes to construct the anomaly forcing, we show here only results using the reanalysis forcing. An additional benefit is that such forcings could also be used in similar experiments with other models.

3. Simulated AMOC: Mean and variability

We show in Fig. 2 the time-mean streamfunction from control simulations of the three models. All show a robust AMOC, with substantial cross-equatorial flow. The AMOC is largest in CM2.1. For each model we compute an index of the AMOC as the maximum value of the annual-mean overturning streamfunction between 20° and 65°N in the North Atlantic. We form time series of the AMOC index for each model. We show the time series and their spectra in Figs. 2d and 2e, respectively. All the spectra are characterized by significant peaks on interdecadal time scales. The peak occurs around 15–20 yr in CM2.1, around 26–30 yr in FLOR, and 30 yr in CM3. By performing identical experiments in models with differing AMOC characteristics, we hope to gain

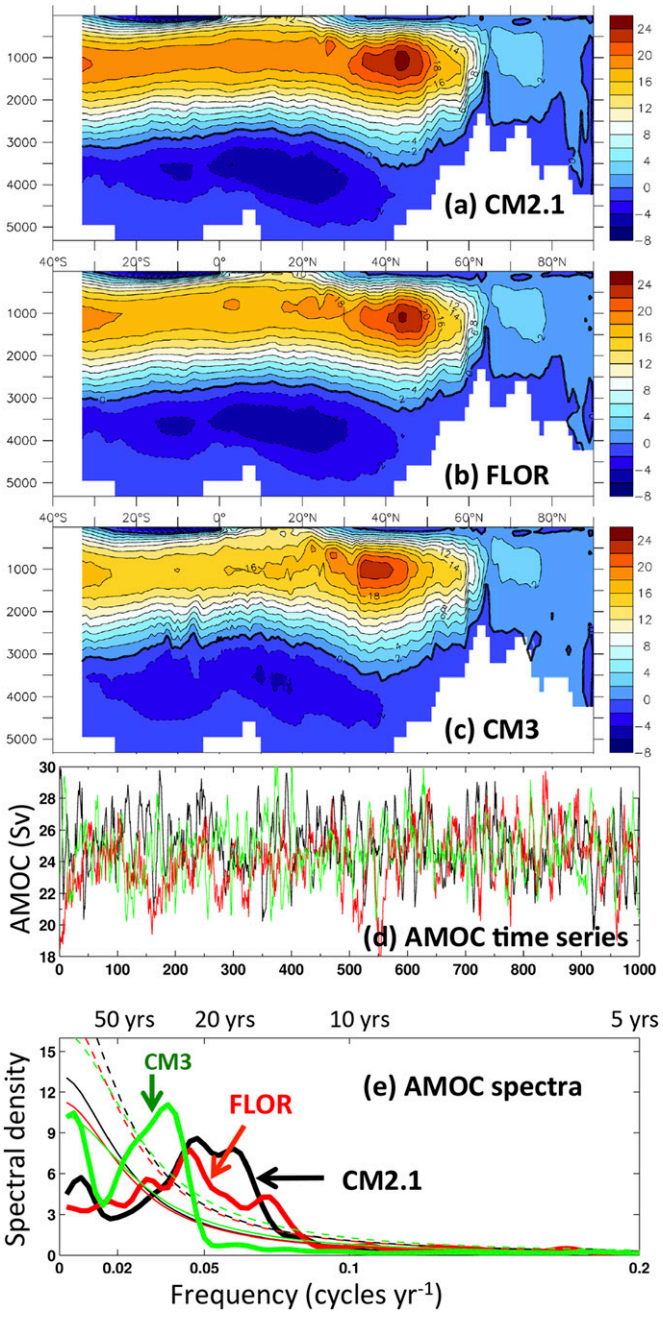

FIG. 2. Streamfunction of zonal-mean Atlantic circulation (Sv) from various models, denoting the mean AMOC in each model: (a) CM2.1, (b) FLOR, and (c) CM3. The flow is along the lines of the streamfunction, with the flow speed proportional to the gradient of the streamfunction. Flow is clockwise around a streamfunction maximum in the latitude–depth plane (depth is in meters). (d) Time series of the AMOC index from each simulation, calculated as the maximum value of the streamfunction each year over 20°–65°N. Black is CM2.1, red is FLOR, and green is CM3. (e) Spectra of the time series of AMOC amplitude in the three models. Black indicates CM2.1, red indicates FLOR, and green indicates CM3. For each model the thick line represents the spectral estimates, the thin solid line is a red noise (first-order Markov process) spectrum fitted to the model spectrum, and the dashed lines represent the 95% confidence interval above the red noise spectrum. The units are frequency along the bottom x axis (cpy) and period in years along the top x axis. The units along the y axis are spectral density (Sv^2 yr).

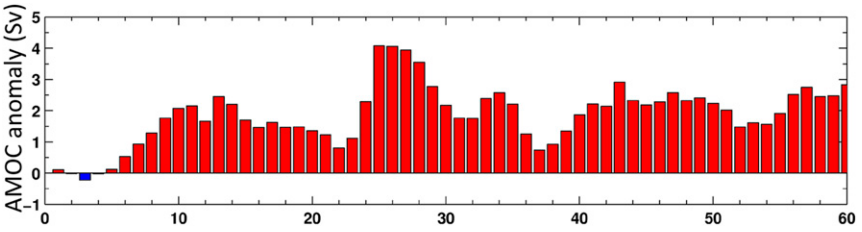

FIG. 3. Ensemble-mean response of the AMOC in CM2.1 to the switch on of NAO-related surface heat fluxes in the North Atlantic. The NAO fluxes are switched on at time 0 yr. The quantity plotted is the maximum streamfunction at 45°N in the experiment with the NAO forcing minus the control simulation.

some measure of the robustness of results. We do not attempt in this study to identify the factors responsible for the differing AMOC characteristics in these models.

4. Response to switch on of NAO forcing

As a first test we use CM2.1 to simulate the response of the AMOC and climate system to suddenly turning on and maintaining an anomalous positive NAO flux forcing whose amplitude corresponds to one standard deviation of the NAO time series. Shown in Fig. 3 is the time series of the response of the AMOC at 45°N to the NAO heat flux forcing. This is computed as the 10-member ensemble-mean AMOC in the NAO flux forcing run minus the 10-member ensemble-mean AMOC from the corresponding control simulation with no externally imposed NAO forcing. The simulated ensemble-mean AMOC adjusts over a decadal scale, increasing in amplitude by several Sverdrups (Sv; 1 Sv $\equiv$ $10^6\,m^3\,s^{-1}$). Physically, the NAO-related fluxes extract heat from the subpolar gyre and Labrador Sea. This increases near-surface density, mixed layer depths, the rate of deep-water formation, and zonal upper-ocean density gradients across the North Atlantic in the latitude range of 45°–75°N. These factors tend to enhance the AMOC (Danabasoglu et al. 2012). Note also that the AMOC response is not steady but varies, with relative maxima around years 10–13 and 25–28. The time scale of these variations is similar to the time scale of internal variability in CM2.1 (15–20 yr as shown in Fig. 2). This similarity of time scales suggests that some of the processes important for the adjustment of the AMOC to this imposed forcing may also be involved in the mechanisms of the dominant time scale of AMOC variability in this model. The response of the model to a switch on of NAO-related fluxes may be a useful way to assess the internal variability time scale of a model and to delineate some of the important processes that control that time scale. This would be most relevant for models in which the NAO plays a dominant role for ocean decadal-scale variability and less relevant for models in which other patterns of atmospheric variability, such as the East Atlantic pattern, are dominant for ocean decadal variability.

We show the spatial structure of this adjustment process in more detail in Fig. 4. This contains the climatological mean of several quantities in the top row from a long control simulation. Subsequent rows show the time-evolving response of those quantities to the imposed NAO forcing, calculated as the ensemble mean of the simulations with the NAO forcing minus the ensemble mean of the simulations without the NAO forcing. Each row from the second row to the bottom denotes a later time after the imposition of the NAO fluxes. The sequence of panels show the adjustment of mixed layer depth, AMOC, northward ocean heat transport, SST, and sea surface salinity (SSS) to the additional NAO flux. The imposed anomalous NAO heat flux in the subpolar gyre and Labrador Sea (see Fig. 1) leads to near-surface cooling and increased mixed layer depths (see the results in the second row from top of Fig. 4 for lag 3, corresponding to 3 years after the imposition of the NAO fluxes). Convection is enhanced along with a slight strengthening of the AMOC. As we move to larger time lags (successively lower rows in Fig. 4) the enhanced mixed layer depths are maintained, the AMOC continues to strengthen, and the region of the enhanced AMOC expands southward. This enhanced AMOC increases ocean heat transport (Fig. 4, center column), leading to positive SST and SSS anomalies throughout the subpolar gyre and portions of the Nordic seas. This tendency continues throughout the first decade.

5. Sensitivity of impact to time scale of forcing

a. *Hemispheric time series*

The switch-on experiment is useful in illustrating the overall response of the AMOC to NAO fluxes, but we

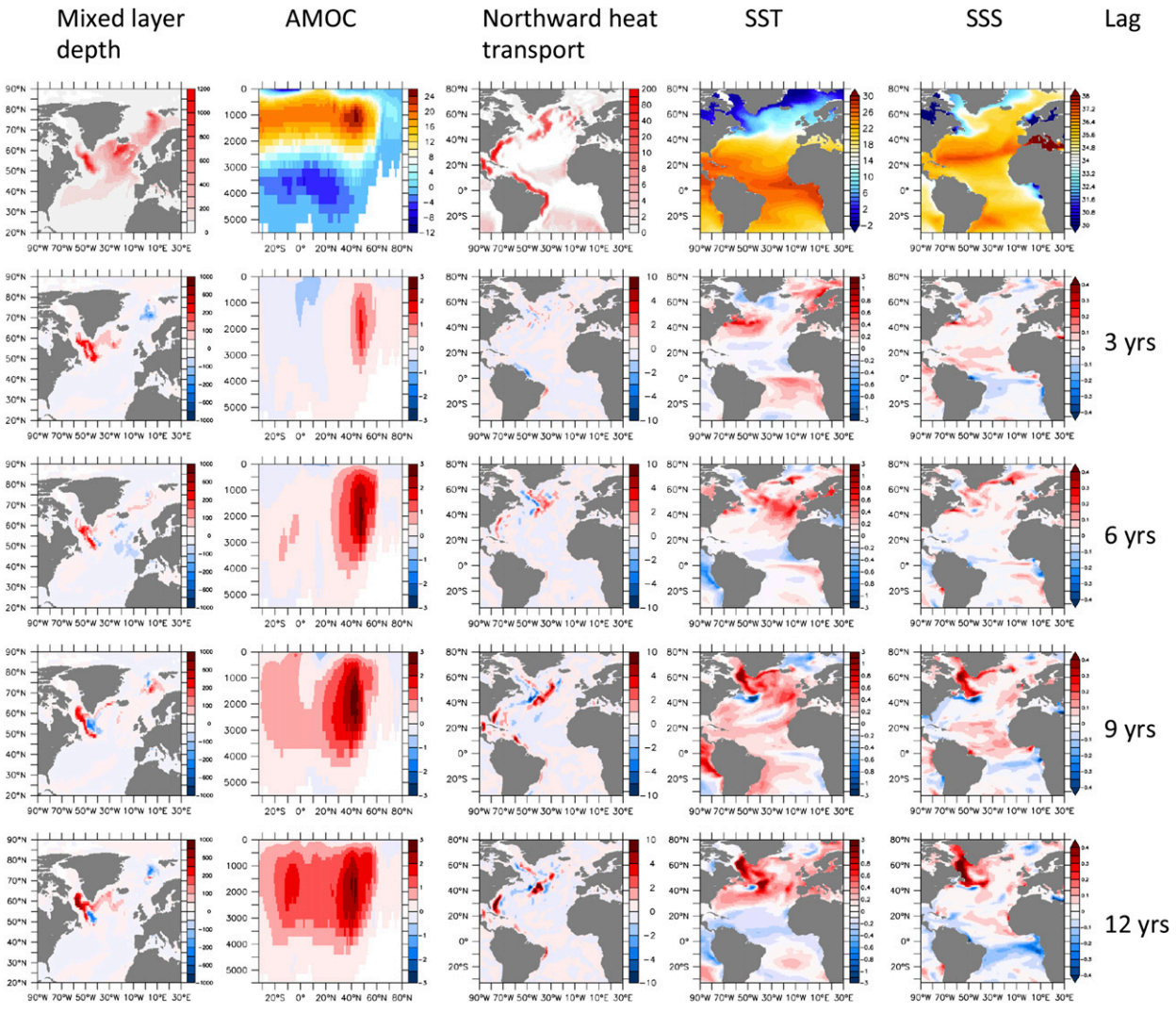

FIG. 4. Adjustment of the North Atlantic in CM2.1 to a sudden switch on of heat flux anomaly corresponding to a one-standard-deviation increase of the NAO. (top)–(bottom) Climatological mean fields for various quantities as noted by labels at the top of each column; rows after (top), anomalies at various times after the switch on of the NAO heat flux. The time is shown on the right, and indicates how much time has passed since the switch on of the NAO-related heat flux forcing. The variables are listed along the top, so that each column corresponds to one variable: (left)–(right) mixed layer depth (m), AMOC (Sv), heat transport (10^{13} W), SST (°C), and SSS (psu).

can also probe this relationship by imposing NAO-related fluxes with well-defined time scales and assessing how the AMOC responds to differing time scales of forcing. Specifically, we create time series of anomalous fluxes that have the spatial pattern of the NAO but whose amplitude is modulated in time by a sine wave with arbitrary periods. We have conducted 10-member ensembles of such experiments with CM2.1 using periodicities of 2, 5, 10, 20, 50, and 100 yr and evaluated the AMOC and climate system response to these forcings. We show in Fig. 5 time series of the AMOC for simulations with various time scales of NAO-related flux forcing. Also shown in each panel (red curve) is the AMOC time series that is calculated as an ensemble average from the 10 corresponding segments of the control simulation. The simulations with shorter time scales of forcing are run for shorter durations. Figure 5a shows simulations with time scales of 2 and 5 yr, in addition to the control. The NAO-induced variability of the AMOC is quite small and is not distinguishable from the mean of the corresponding segments of the control. Figure 5b shows results from forcings with periodicities of 10 and 20 yr. There is a substantial increase in the response of the AMOC to the forcing, particularly for the 20-yr time scale. Figure 5c shows results from forcing at time scales of 50 and 100 yr. The AMOC fluctuates at the time scale of the forcing, but the amplitude is similar to that at 20 yr.

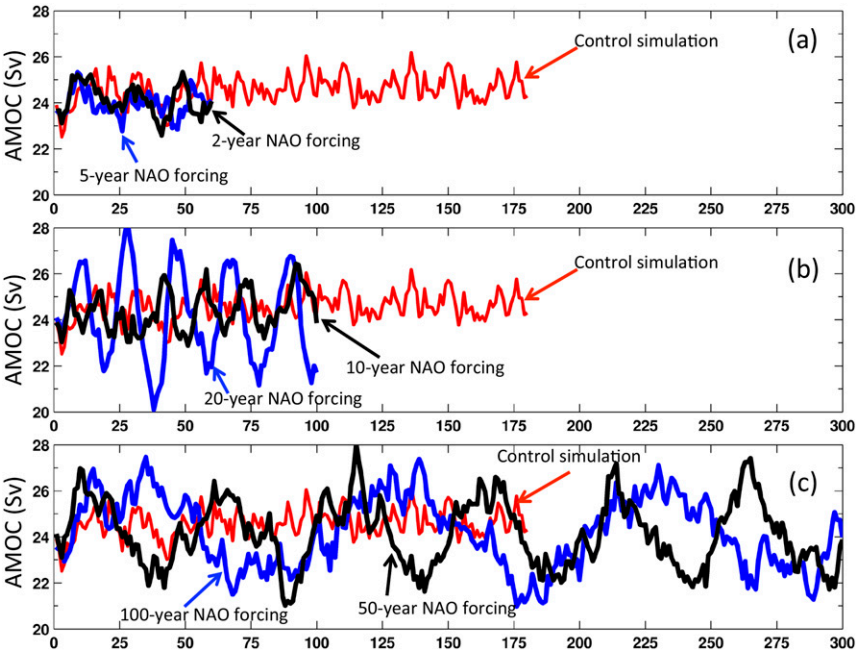

FIG. 5. Time series of AMOC index (defined as the maximum streamfunction value each year over the domain 20°–65°N) for various experiments using CM2.1. The red curve in each panel shows values from the reference control simulation, calculated as the ensemble mean over 10 segments of the control simulation that correspond to the 10 ensemble members of the perturbation experiments. (a) Black (blue) curve shows 10-member ensemble-mean AMOC from simulations with NAO forcing at a time scale of 2 (5) yr. (b) Black (blue) curve shows 10-member ensemble-mean AMOC from simulations with NAO forcing at a time scale of 10 (20) yr. (c) Black (blue) curve shows 10-member ensemble-mean AMOC from simulations with NAO forcing at a time scale of 50 (100) yr.

We can characterize the response at each time scale by the standard deviation of the ensemble-mean AMOC time series. Figure 6a shows the standard deviation of the AMOC as a function of the time scale of the forcing. It is clear that the response is small at short time scales of forcing and increases until reaching a time scale close to the characteristic internal time scale of the model AMOC variability (~20 yr). The amplitude of the AMOC response does not substantially vary as we further increase the time scale of the forcing. The largest response at a time scale of 20 yr may be indicative of a resonant response of the system when forced at the preferred time scale of variability. We show in Fig. 6b the same quantity for ocean heat transport at 23°N summed over all longitudes and note very similar behavior (the response in the Pacific Ocean is small, so we obtain essentially the same result if we compute ocean heat transport only in the Atlantic Ocean).

We expect that variations in the AMOC and oceanic heat transport may influence extratropical Northern Hemisphere surface air temperature (NHSAT) and Northern Hemisphere sea ice mean thickness (NHSI). NHSAT is computed by averaging annual-mean surface air temperature for all model points poleward of 23°N, and NHSI is calculated by averaging annual-mean sea ice thickness poleward of 55°N. We show in Figs. 6c and 6d the amplitudes of variations of NHSAT and NHSI, respectively. We note that, as was the case with the AMOC and heat transport, variations are small at short time scales and increase up to 20 yr. However, in contrast to the AMOC, the amplitude of NHSAT and NHSI variations continues to increase with the time scale of the forcing, such that the amplitude of the response for NHSI at a 100-yr forcing time scale is 2–3 times the amplitude of the response for forcing at 20 years. Why is there a continued increase in the amplitude of the NHSAT and NHSI variations when the amplitudes of the AMOC and oceanic heat transport variations are approximately constant for time scales longer than 20 years? There are multiple contributing factors. First, the time integral of the ocean heat transport anomalies is important for the climate response; this time integral is approximately 3 times larger for the 100-yr forcing than for the 20-yr forcing, leading to a larger response. In addition, in response to a warming of the climate system there is reduced snow cover and sea ice, thereby leading

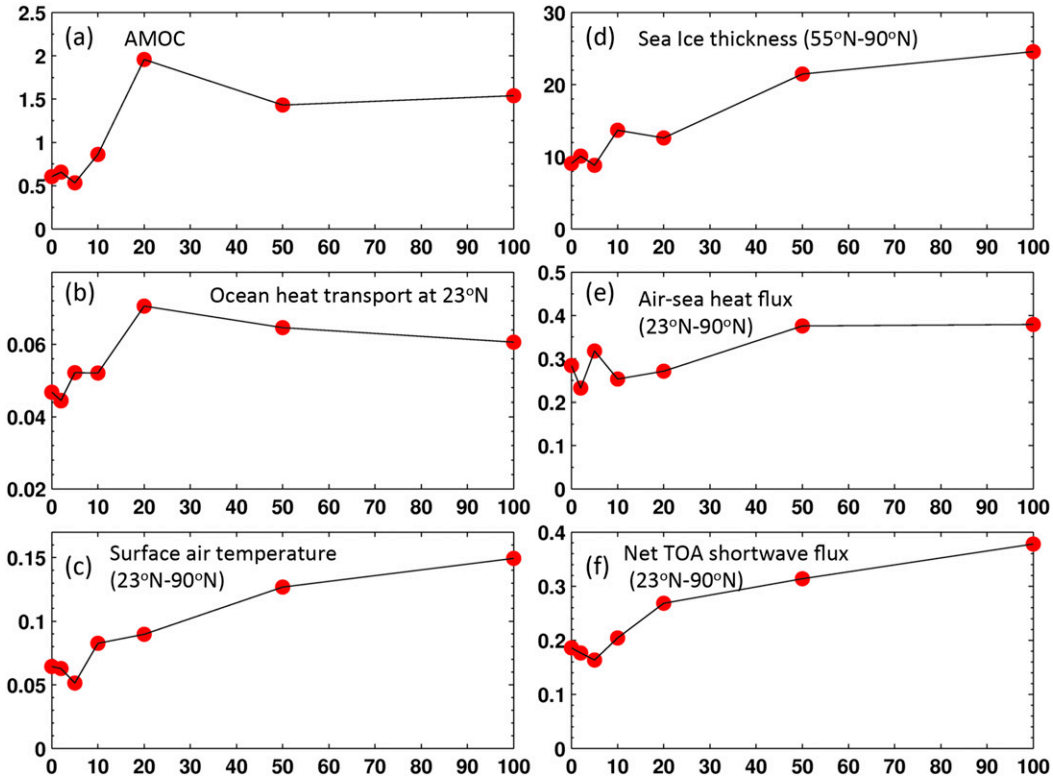

FIG. 6. (a) Each circle represents the standard deviation of the ensemble-mean AMOC time series from a perturbation experiment using NAO forcing at a particular time scale. The values along the *y* axis indicate the value of the standard deviation, while the values along the *x* axis indicate the time scale (yr) of the NAO forcing for each experiment. (b) As in (a), but for meridional ocean heat transport (10^{15} W) at 23°N (summed over all longitudes). (c) As in (a), but for annual-mean surface air temperature (K) averaged over all points poleward of 23°N. (d) As in (a), but for annual-mean sea ice thickness (cm) averaged over all points poleward of 55°N. (e) As in (a), but for air–sea surface heat flux (W m^{-2}) averaged over all points poleward of 23°N. (f) As in (a), but for net upward shortwave radiation at the top of the atmosphere (W m^{-2}), averaged over all points poleward of 23°N.

to a positive albedo feedback. This amplifies the signal at longer time scales, which is already larger as a result of the larger time integral of the heat transport changes. Shown in Figs. 6e and 6f are the amplitudes of the variations of the air–sea heat flux and the net upward shortwave radiation at the top of the atmosphere, respectively (both quantities are averaged from 23° to 90°N). The amplitude of the variations of these terms continues to grow for time scales longer than 20 yr, indicating that these play an increasingly important role at longer time scales.

To more clearly illustrate these relationships we show in Fig. 7 the time series of various quantities for two sets of simulations with NAO forcing time scales of 20 yr (black curves) and 100 yr (red curves). The responses of the AMOC and ocean heat transport have similar amplitudes for the two time scales of forcing, consistent with Fig. 6.

The larger response of surface air temperature for the 100-yr time-scale forcing relative to the 20-yr time-scale forcing is apparent in Fig. 7c. The amplitude of the response is significantly larger, and the variance of the temperature response is approximately 3 times larger for the 100-yr forcing than for the 20-yr forcing. Shown in Fig. 7d are similar curves for Arctic mean sea ice thickness; the variance increases by more than a factor of 3 between the 20-yr forcing and the 100-yr forcing, despite similar (or even smaller; see Figs. 6a,b) amplitudes of AMOC and oceanic heat transport variations at 100 years relative to 20 years. These results suggest that the climatic relevance of NAO-induced AMOC variations increases substantially with time scale. The larger amplitude of the temperature response at longer time scales is at least partially attributable to the greater role of feedbacks in the system. At high latitudes the cryosphere responds to the warming or cooling induced by AMOC variations, and these cryospheric changes in turn influence the amount of shortwave radiation reflected to space, acting as a positive feedback on the system. The time series of anomalies of upward

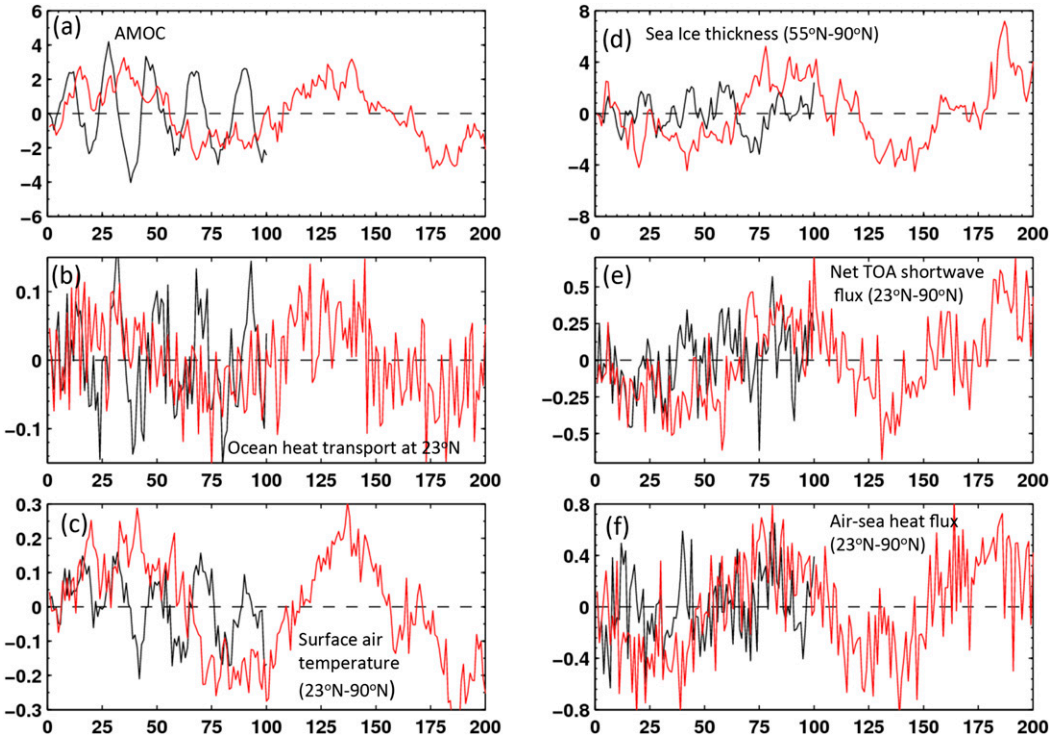

FIG. 7. Time series of various quantities in model simulations driven by a periodic NAO heat flux forcing. Shown are the results from a 20-yr time scale NAO forcing experiment (black) and a 100-yr time scale NAO forcing (red). Each time series is the 10-member ensemble mean of the NAO forced experiment minus the corresponding control simulation. The 20-yr (100 yr) forcing experiments are 100 (200) years in duration: (a) AMOC index (Sv), (b) meridional ocean heat transport (10^{15} W) at 23°N, (c) surface air temperature (K) averaged over all points poleward of 23°N, (d) annual-mean sea ice thickness (cm) averaged over all points poleward of 55°N, (e) annual-mean net upward shortwave radiation at the top of the atmosphere (W m^{-2}) averaged over all points poleward of 23°N and (f) ocean–atmosphere heat flux (W m^{-2}) averaged over all points poleward of 23°N.

shortwave radiation at the top of the atmosphere are shown in Fig. 7e; the variance increases by a factor of 1.5 from the 20-yr forcing to the 100-yr forcing. This positive albedo feedback is more effective at longer time scales as progressively more of the cryosphere is altered by the NAO-induced AMOC changes and therefore participates in the positive feedback. We also show the time series of average air–sea heat flux poleward of 23°N in Fig. 7f. The variance of the air–sea heat flux time series also increases in the 100-yr forcing case relative to the 20-yr forcing case by a factor of 2. As the amount of sea ice decreases, more open ocean is available to flux heat more effectively from the ocean to the atmosphere; since the sea ice extent is more powerfully impacted on longer time scales, this air–sea heat flux term is also stronger for longer time scales. However, this term is somewhat limited by the total anomalous heat transport in the ocean.

The above suggests that NAO-induced changes in the AMOC create changes in ocean heat transport that drive hemispheric-scale variations in surface air temperature and sea ice. In addition, the effect becomes much stronger at long time scales because of the greater time integral of the ocean heat transport changes and feedback processes associated with changes in snow cover and sea ice.

b. *Heat budget diagnostics*

We next examine in Fig. 8 the changes in oceanic and atmospheric heat transport, as well as changes in the top-of-the-atmosphere radiation balance, generated by the simulations with 100-yr NAO flux forcing using CM2.1 (results from the 50-yr forcing simulations are similar). In Fig. 8a we plot the linear regression coefficients of the time series of the NAO forcing with itself at various lags; this provides a visual perspective for interpreting the phasing of the changes shown in Figs. 8b,c. We show in Fig. 8b the linear regression coefficients of poleward oceanic heat transport at 50°N (integrated over all depths) versus the NAO flux forcing time series at various lags (where negative lags refer to times before a maximum of the NAO forcing). We find

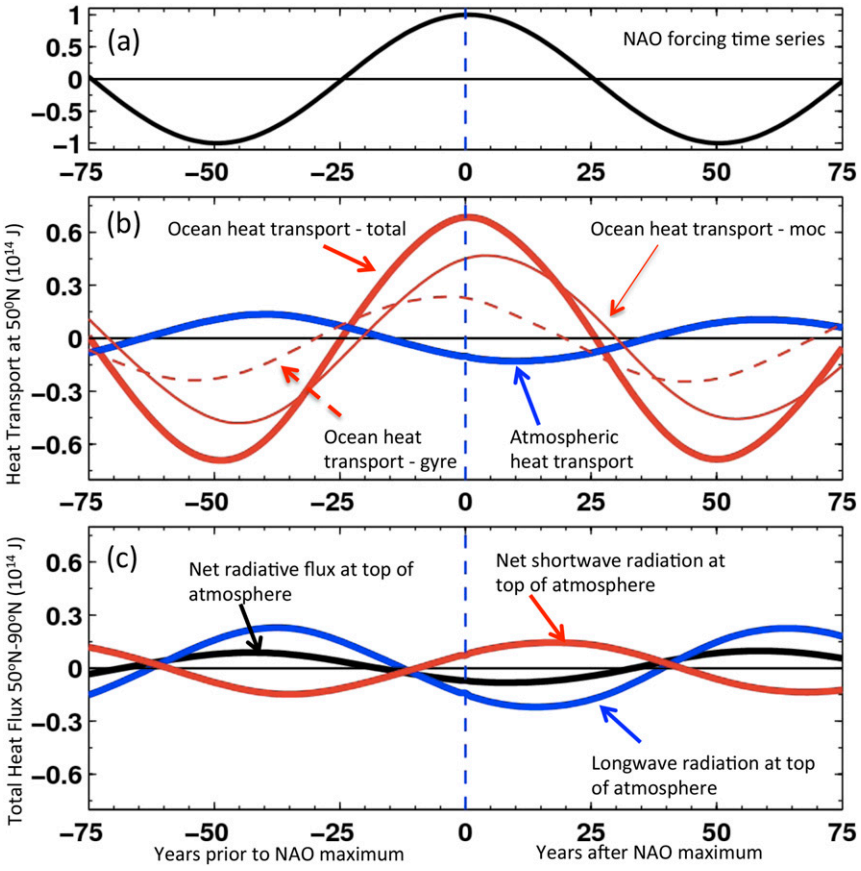

FIG. 8. (a) Regression of time series of imposed NAO forcing vs itself. (b) Regression of changes in oceanic (Atlantic only) and atmospheric (all longitudes) heat transport at 50°N vs the NAO forcing. Time is along the x axis in years. Negative (positive) values indicate years before (after) the imposed NAO maximum. A regression value of +1.0 would indicate an enhanced poleward oceanic heat transport of 10^{14} J. Thick red line is for total poleward oceanic heat transport, thin red line for the meridional overturning component (moc) of the transport, and dashed line for the gyre component of the transport. Blue line is poleward atmospheric heat transport at 50°N. (c) Regression of changes in net incoming radiation at the top of the atmosphere vs the NAO time series, integrated over all regions poleward of 50°N. Positive values indicate an increase in the flux of radiation from space to Earth (i.e., a heating of the climate system). Red denotes net shortwave radiation, blue denotes longwave radiation, and black denotes the net radiative flux (10^{14} J). For example, negative values of longwave radiation for years 0–30 after the NAO forcing indicate an increase of outgoing longwave radiation to space as a response to warming of the Northern Hemisphere associated with the increased poleward oceanic heat transport shown in (b).

that variations in Pacific transport (not shown) are extremely small compared to changes in Atlantic heat transport, and so we show only changes in Atlantic heat transport. The ocean heat transport variations are in phase with the NAO flux forcing. We also show that changes in poleward atmospheric heat transport are smaller in amplitude and opposite in sign to the ocean heat transport changes, consistent with the idea of Bjerknes compensation (Bjerknes 1964; Shaffrey and Sutton 2006; Yang et al. 2013). The atmospheric heat transport changes act as a negative feedback on the system. Enhanced (reduced) ocean heat transport warms (cools) the higher latitudes, thereby reducing (increasing) the meridional temperature gradient in the atmosphere and decreasing (increasing) the poleward atmospheric heat transport.

We next decompose the ocean heat transport variations into gyre and overturning components, calculated using monthly data at each model level:

$$mC_pVT = mC_p(V'T + \overline{V}T), \tag{1}$$

where m denotes the mass of water, C_p is the heat capacity of seawater, V denotes meridional velocity in the

ocean, T is ocean temperature, the overbar denotes the zonal mean across the Atlantic, and the prime denotes the deviation from that zonal mean. We calculate linear regressions between these heat transport components and the NAO forcing and show these in Fig. 8b. The overturning component [second term on right-hand side of (1), labeled moc in Fig. 8b] dominates the total heat transport changes, but there is still a significant role for gyre variations [first term on right-hand side of (1)]. The gyre changes appear to lead the overturning changes.

In Fig. 8c we show the regression coefficients of changes in the top-of-the-atmosphere radiation balance versus the NAO forcing (where the radiation terms are calculated as the integral for all points poleward of 50°N). The net radiation at the top of the atmosphere lags the ocean heat transport and is a negative feedback. Variations in outgoing longwave radiation and net shortwave radiation (netsw) are also shown. It is clear that enhanced (decreased) ocean heat transport warms (cools) the high latitudes, which then emit more (less) longwave radiation to space. This dominates the radiation variations. However, the netsw term acts as a positive feedback. Physically, warming (cooling) of the higher-latitude regions reduces (increases) the amount of sea ice and snow cover, thereby reducing (increasing) albedo and increasing (decreasing) the amount of shortwave radiation absorbed in the system. This shortwave feedback opposes the damping by longwave radiation and therefore helps to amplify the warming signal. This is more pronounced at longer time scales of forcing.

The larger response at longer time scales is partially attributable to greater amplification from shortwave radiation forcing. In addition, the time integral of the ocean heat transport is considerably larger for the 100-yr NAO forcing than for shorter time scales, since the anomalous ocean heat transport is maintained for a longer period. The time integral of the anomalous poleward oceanic heat transport reaches a maximum of 2.31×10^{22} J for the 20-yr NAO forcing versus a maximum of 6.62×10^{22} J for the 100-yr NAO forcing. This substantially larger time integral of heating translates into considerably larger climatic impacts, as shown in Fig. 6 and below.

c. *Spatial patterns of response*

We show in Figs. 9–13 the spatial patterns of the responses to the NAO-induced AMOC variations. The responses are computed as the linear regression of the time series of the response for each variable (forced experiment minus control) versus the time series of anomalous NAO flux forcing and are scaled such that the values shown represent the response to a two-standard-deviation NAO forcing (meant to illustrate the difference between a one-standard-deviation positive NAO phase and a one-standard-deviation negative NAO phase). We note that, for simplicity, we are using a fixed spatial pattern of the NAO, whereas in reality this pattern changes in time. The responses for the January–March (JFM) season for both time scales of forcing are in Figs. 9 and 10 and for July–September (JAS) in Figs. 11 and 12. These months are chosen to emphasize responses in winter and summer sea ice as well as changes in precipitation and tropical atmospheric circulation of relevance for tropical cyclone development. We show maps corresponding to the lags of maximum response in extratropical mean surface air temperature.

The Northern Hemisphere (NH) cold season responses for the two time scales are shown in Figs. 9 and 10 and display a clear sensitivity to time scale. Surface air temperature changes (Figs. 9a,e) show warming at high latitudes, but the warming is larger and more extensive for the 100-yr forcing. In particular, the warming signal extends over most of the Eurasian continent in the 100-yr forcing case but is largely confined to oceanic regions of the North Atlantic and Arctic in the 20-yr forcing case. The precipitation response is shown in Figs. 9b,f. There is a general increase in precipitation over the North Atlantic for both time scales in response to the generally warmer upper ocean. One exception is the notable decrease off the northeast coast of North America in the 20-yr forcing case. This is associated with local cooling related to a southward shift of the recirculation gyre (Zhang and Vallis 2007). This effect is muted at the 100-yr time scale where the warming of the North Atlantic is more pervasive. The changes in SLP are shown in Figs. 9c,g. In both cases there is reduced SLP over the North Atlantic, but the larger-scale structure over the Northern Hemisphere differs between the two cases. On the longer time scale there is a tendency for reduced SLP over the entire regions of the North Atlantic and the Arctic, whereas there is a more structured pattern at the shorter time scale. In the upper troposphere (Figs. 9d,h) there is a structured response at the shorter time scale of forcing, with regions of increases and decreases, but a more uniform increase in geopotential heights across the Northern Hemisphere at the longer time scale.

The sea ice changes for the JFM season are shown in Fig. 10. For the 20-yr forcing sea ice changes are confined to the Labrador Sea and Nordic seas, but the changes extend over the entire Arctic for the 100-yr forcing case.

We show in Fig. 11 results for the JAS season. The contrasts in the response of surface air temperature and sea ice thickness between the two time scales of forcing

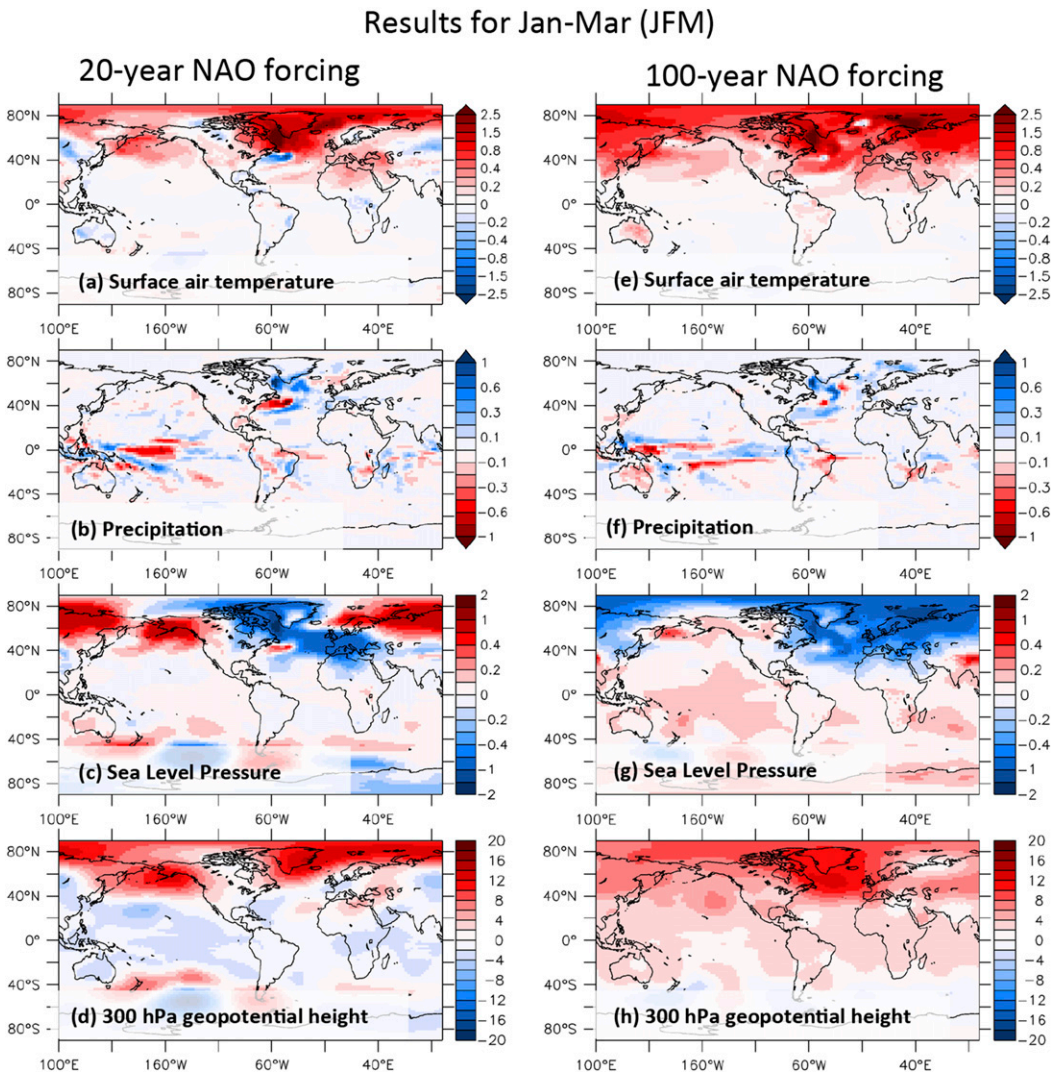

FIG. 9. Spatial patterns of simulated response to NAO-related surface heat flux anomalies. The responses are averaged over JFM. Results are shown from simulations with (a)–(d) 20-yr and (e)–(h) 100-yr NAO forcing. Values plotted are regression coefficients of the various fields vs the imposed NAO time series, normalized to represent the response to a two-standard-deviation change in the NAO. Results in (a)–(d) are shown for a 20-yr time scale of flux forcing, showing fields 7 years after maximum of imposed NAO flux forcing. Results in (e)–(h) are shown for a 100-yr time scale of flux forcing, plotted 13 years after maximum of imposed NAO flux forcing.

is similar to the winter season. The summer precipitation response is shown in Figs. 11b,g. Consistent with previous work, the stronger AMOC leads to a northward migration of the intertropical convergence zone (ITCZ) and associated rainfall, particularly over the African–Atlantic sector (Vellinga and Wu 2004; Zhang and Delworth 2005). This effect is considerably stronger in response to the 100-yr forcing. For sea level pressure there is more consistency in the responses between the time scales, with reduced SLP over the North Atlantic and Arctic. This reduction in SLP over the Atlantic is consistent with analyses of the instrumental record (Sutton and Hodson 2005). Changes in 300-hPa geopotential height are shown in Figs. 11d,i—the difference is striking. For the 20-yr forcing there is a modest impact, but for the 100-yr forcing there is a widespread increase of geopotential heights over the Northern Hemisphere, extending as far south as 40°S. These changes in geopotential height are consistent with the changes in the vertical shear of the zonal wind (hereafter referred to as shear), shown in Figs. 11e,j. There is a substantial reduction in shear over the tropical and subtropical North Atlantic in the 100-yr forcing case, with a generally smaller overall impact for the 20-yr case. This suggests that NAO-induced AMOC changes would substantially influence tropical storm activity for

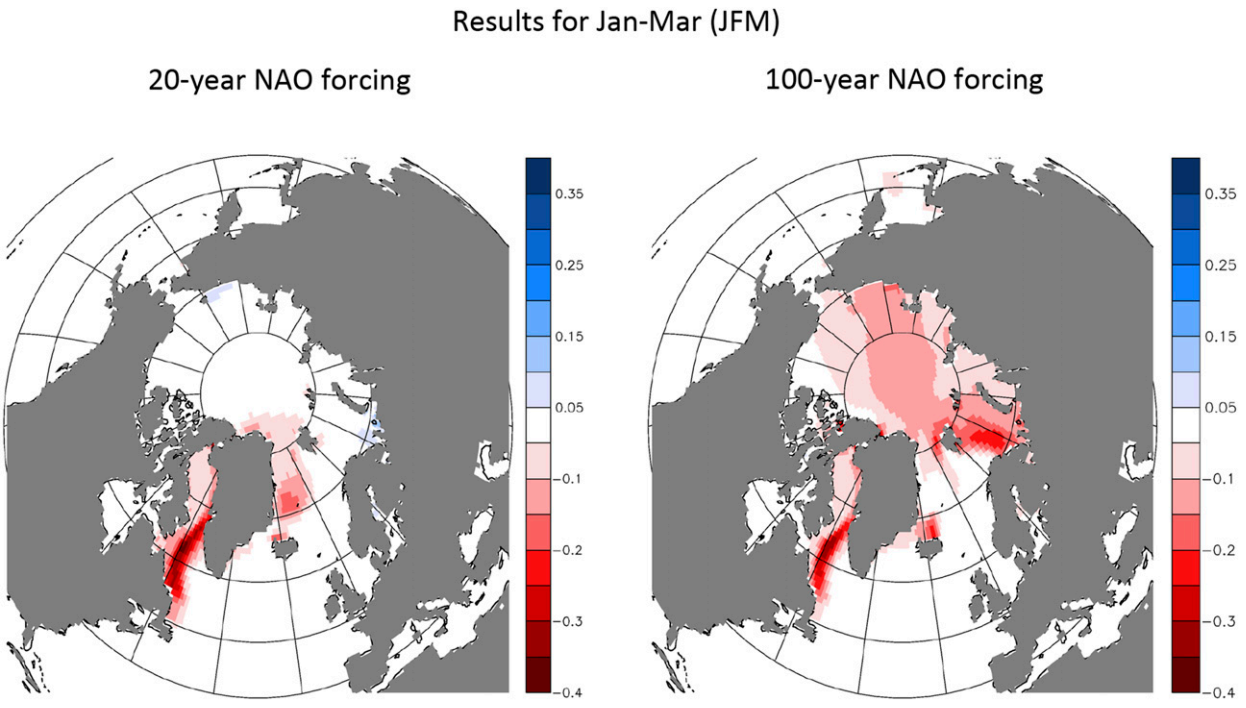

FIG. 10. As in Fig. 9, but for sea ice thickness. Units are meters per two-standard-deviation NAO forcing.

the 100-yr forcing case, although the model used for this study does not have sufficient resolution to explicitly simulate tropical storms.

The sea ice response for JAS is shown in Fig. 12. While there is very little impact for the 20-yr forcing case, there is a pan-Arctic reduction in sea ice thickness for the 100-yr forcing case.

We show in Fig. 13 the changes in sea surface height induced by the NAO forcing. As shown previously, the AMOC increases in response to positive NAO forcing; this is consistent with an enhanced zonal gradient in sea level height, with negative anomalies along the North American coast and positive anomalies in the mid-Atlantic. These results suggest that decadal-scale variations in the NAO induce decadal-scale sea level changes (Goddard et al. 2015; McCarthy et al. 2015) along portions of the eastern coast of North America, with short-term trends in sea level change of up to 10 cm decade^{-1}. Note that sea level heights along the east coast of North America tend to fall in response to a sustained positive NAO and rise in response to a sustained negative NAO. This process can therefore contribute substantially to local decadal-scale sea level variations. Additional analyses show that the pattern of sea level height changes propagates to the southwest, more rapidly with the 20-yr NAO forcing than the 100-yr NAO forcing. The amplitude of the sea level changes is similar for the 20- and 100-yr forcing cases, consistent with similar changes in the AMOC for the two forcing cases. In terms of rates of change in sea level, this implies that the 20-yr forcing would have a much greater impact on decadal-scale changes in sea level than the 100-yr forcing. Their spatial structures differ somewhat, with more of the changes extending through the Labrador Sea and into Baffin Bay for the 100-yr forcing. Both patterns, however, are consistent with modulation of the zonal gradient of sea level, consistent with AMOC variations.

6. Sensitivity of impact to model and mean base state

The previous sections examined how the response of the AMOC and larger-scale climate to NAO variations depends on the time scale of the NAO forcing using a single model (CM2.1). In this section we explore how the response to NAO forcing depends on the model's characteristics, including its mean state. We make use of two additional models, FLOR and CM3, as described in section 2a. For all three models we conduct switch-on experiments in which heat fluxes corresponding to a positive phase of the NAO are suddenly applied to the model ocean. These simulations are 60 years in duration, with the anomalous flux forcing held constant (but applied only in the months of December–March). Using this simple model design, we wish to compare the

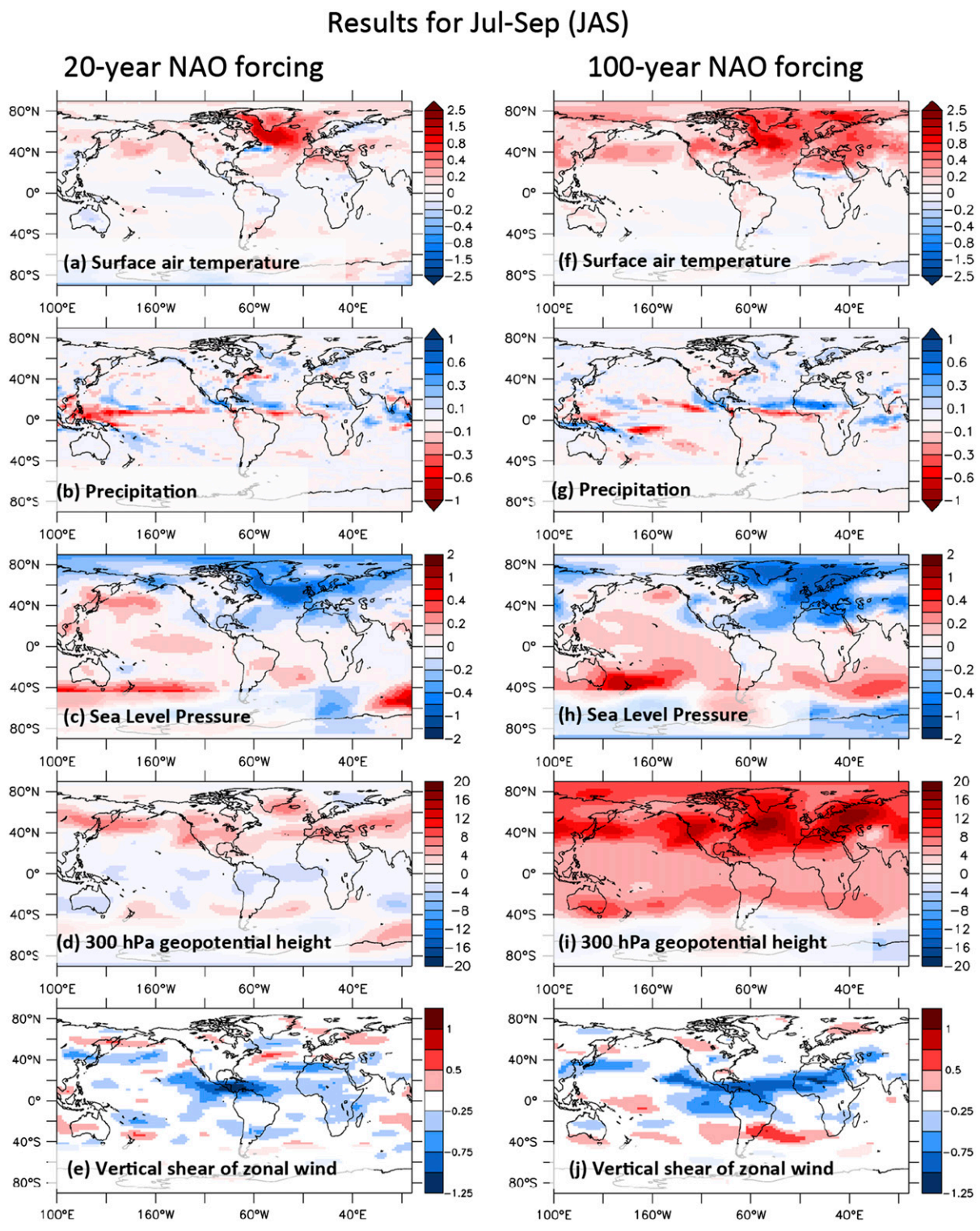

FIG. 11. Spatial patterns of simulated response to an increase in the AMOC induced by NAO-related surface heat flux anomalies. The responses are averaged over JAS. Results are shown from simulations with (a)–(e) 20- and (f)–(j) 100-yr NAO forcing. Values plotted are regression coefficients of the various fields vs the time series of the heat flux forcing; these are normalized to represent the response to a two-standard-deviation change in the NAO-induced fluxes. Results in (a)–(e) are shown for a 20-yr time scale of flux forcing, showing fields 7 years after maximum of imposed NAO flux forcing. Results in (f)–(j) are shown for a 100-yr time scale of flux forcing, plotted 13 years after maximum of imposed NAO flux forcing. The vertical shear of the zonal wind in (e),(j) is calculated as the zonal wind at 250 hPa minus the zonal wind at 850 hPa.

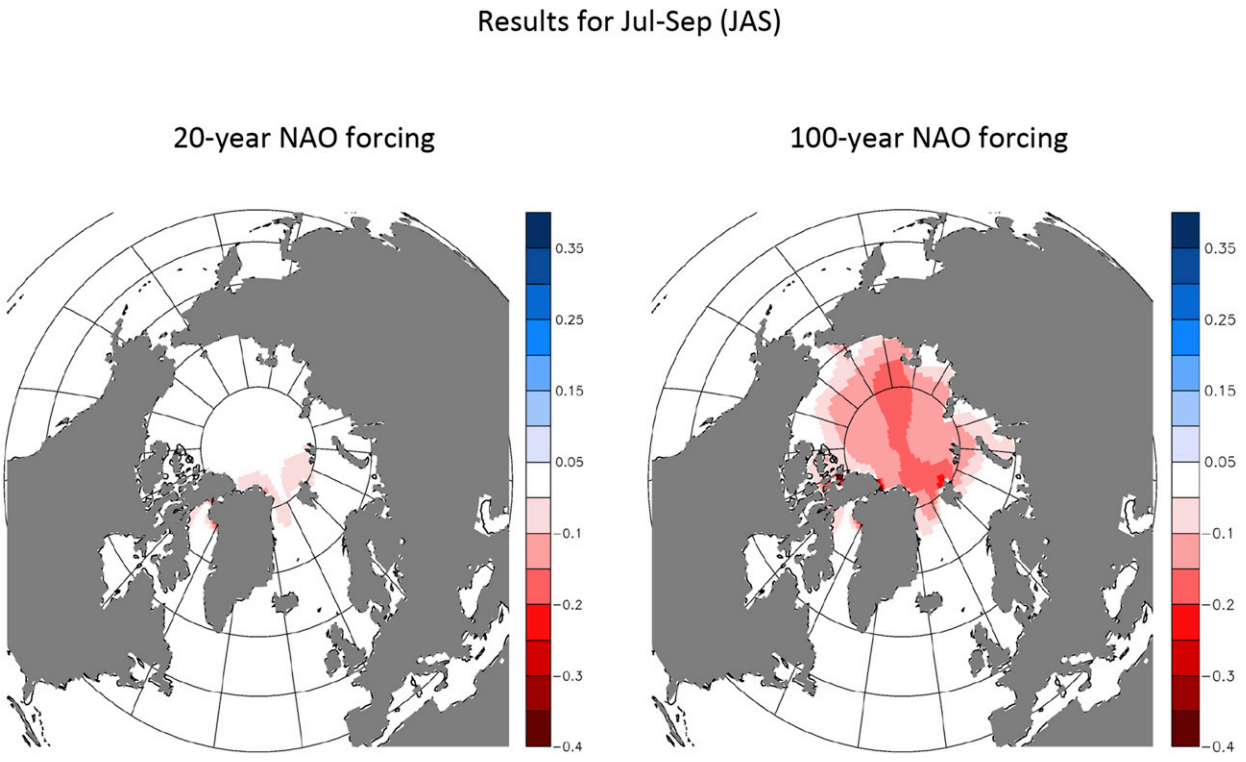

FIG. 12. As in Fig. 11, but for sea ice thickness. Units are meters per two-standard-deviation NAO forcing.

AMOC and climatic responses among the three models. We conduct 10-member ensembles for CM2.1 and 5-member ensembles for FLOR and CM3 (we use smaller ensembles for FLOR and CM3 because of the greater computational cost of the higher-resolution models).

We show in Fig. 14 the AMOC and surface air temperature responses for the three models. All have an increase in AMOC and zonal-mean surface air temperature in response to the switch on of the NAO forcing, but there are modest differences in the time scale and amplitude of the response. Part of this may be due to sampling issues, and part may be due to the differing physical characteristics of each model.

The overall amplitude of the temperature response is largest in FLOR, possibly related to the thicker and more extensive sea ice in the climatological mean state of FLOR (not shown), especially in the Labrador Sea, Barents Sea, and Nordic seas. This offers the potential for greater albedo feedback and temperature response. While CM3 has the longest time scale of internal AMOC variability among the three models (see spectral analysis in Fig. 2), it appears to respond the most rapidly to the switch on of the NAO forcing. In comparing CM2.1 and FLOR, the AMOC response appears to fluctuate on a longer time scale in FLOR compared to CM2.1, consistent with the longer time scale of internal variability in FLOR (see Fig. 2). Despite the above differences, the overall characteristics of the responses are similar, suggesting some degree of robustness in the response.

We also compare the models in their response to a periodic NAO forcing. We select a 50-yr time-scale NAO forcing for the comparison. Based on the results of the previous section, the response at 20-yr forcing was somewhat muted and therefore not a good choice for the comparison. In addition, the computational cost of performing 100-yr forcing experiments was substantial for the higher-resolution FLOR and CM3 models, so we choose to do the comparison at the intermediate time scale of 50 yr.

We show in Fig. 15 responses for the AMOC and surface air temperature (the ocean heat transport response is similar to the AMOC response). The results show broad similarities between the models, with differences in the details of the amplitude and characteristics of the response. The AMOC response is broadly similar between CM2.1 and FLOR, although the CM2.1 response at this time scale is more limited in duration than in FLOR. The shorter internal time scale for the AMOC in CM2.1 suggests that negative feedbacks associated with the oscillatory behavior kick in more rapidly, limiting the response of the AMOC in each phase of the NAO forcing. The response in FLOR to the same forcing is more persistent, consistent with the longer time scale of internal variability. The surface air

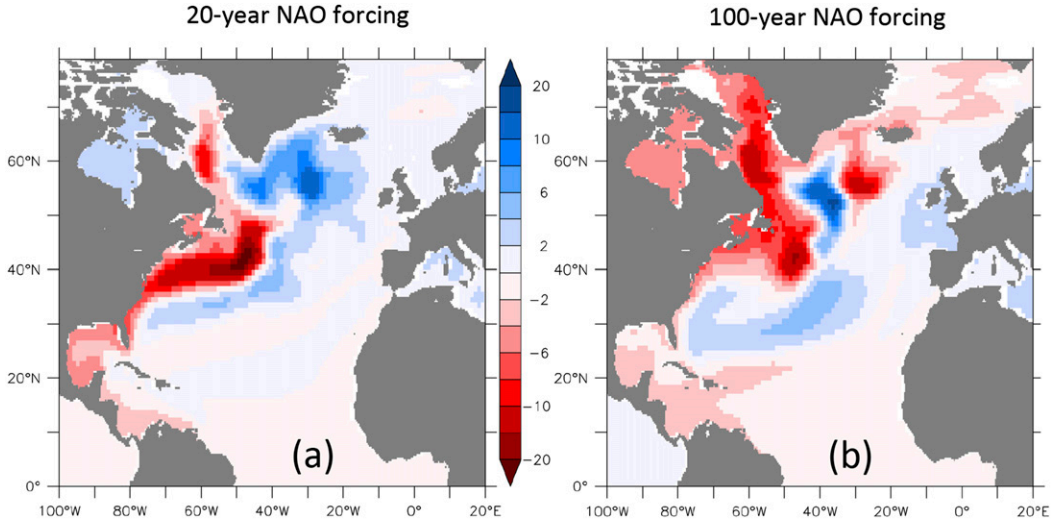

FIG. 13. Regression of annual-mean sea level height anomaly vs the time series of NAO forcing, expressed as the difference in centimeters between a positive one-standard-deviation NAO forcing and a negative one-standard-deviation NAO forcing. For both cases the maps are representative of conditions 6 years after the maximum NAO flux forcing. (a) Case with NAO forcing at 20 years. (b) Case with NAO forcing at 100 years.

temperature results are consistent with the AMOC results, with perhaps somewhat more noise in the responses (cf. the temperature response in CM2.1 and FLOR to their respective AMOC responses, and it is apparent that the temperature response has more noise).

Given this spread among the models in their response to the NAO forcing, particularly for temperature, we compute a multimodel mean response to the NAO forcing and show this in Fig. 16. We see a well-defined and coherent AMOC response to the NAO forcing, with a response amplitude of approximately 2 Sv (corresponding to a one-standard-deviation change in the NAO). This corresponds to an approximately 0.2-K amplitude response of extratropical NH mean surface air temperature to a one-standard-deviation change in the NAO. For a 50-yr time scale of forcing, this implies a trend in extratropical hemispheric temperature of 0.4 K $(25\,\mathrm{yr})^{-1}$.

7. Summary and discussion

This work systematically explores the impact of interannual- to centennial-scale variations in the NAO on the climate system through the effect of NAO-related surface heat fluxes on the ocean. The large-scale climatic impacts arise through NAO-induced changes to the ocean that, in turn, modify the rest of the climate system. We have conducted suites of experiments with multiple climate models in which we artificially impose extra heat flux anomalies on the model ocean in the North Atlantic. The heat flux anomalies have the spatial structure of the NAO but are modified such that their areal integral is zero, meaning that there is no net addition of heat to the coupled system.

In its positive phase, NAO fluxes remove more heat than usual from the ocean in the subpolar and subtropical North Atlantic while removing less heat than usual from the western Atlantic and eastern Nordic seas. The enhanced removal of heat from the subpolar gyre and Labrador Sea increases near-surface density and mixed layer depths, thereby enhancing deep-water formation and horizontal density gradients, leading to an enhanced AMOC and associated poleward oceanic heat transport (Danabasoglu et al. 2012). By conducting simulations with multiple models in which the NAO-related fluxes are instantaneously switched on and maintained indefinitely in a positive NAO phase, we find that there is an approximate decadal-scale adjustment process in which the AMOC strengthens.

We conduct suites of experiments in which we subject the model to sinusoidally varying NAO-related fluxes, similar to Visbeck et al. (1998). In simulations with NAO forcing periods ranging from 2 to 100 yr, we see that the model AMOC has very little response to forcing at time scales shorter than a decade or so. The adjustment processes by which the AMOC responds to NAO forcing are on the order of one decade, so forcing on shorter time scales is not able to significantly influence the AMOC. At longer time scales the AMOC varies largely in phase with the forcing, although it exhibits some preference for forcing close to the dominant time

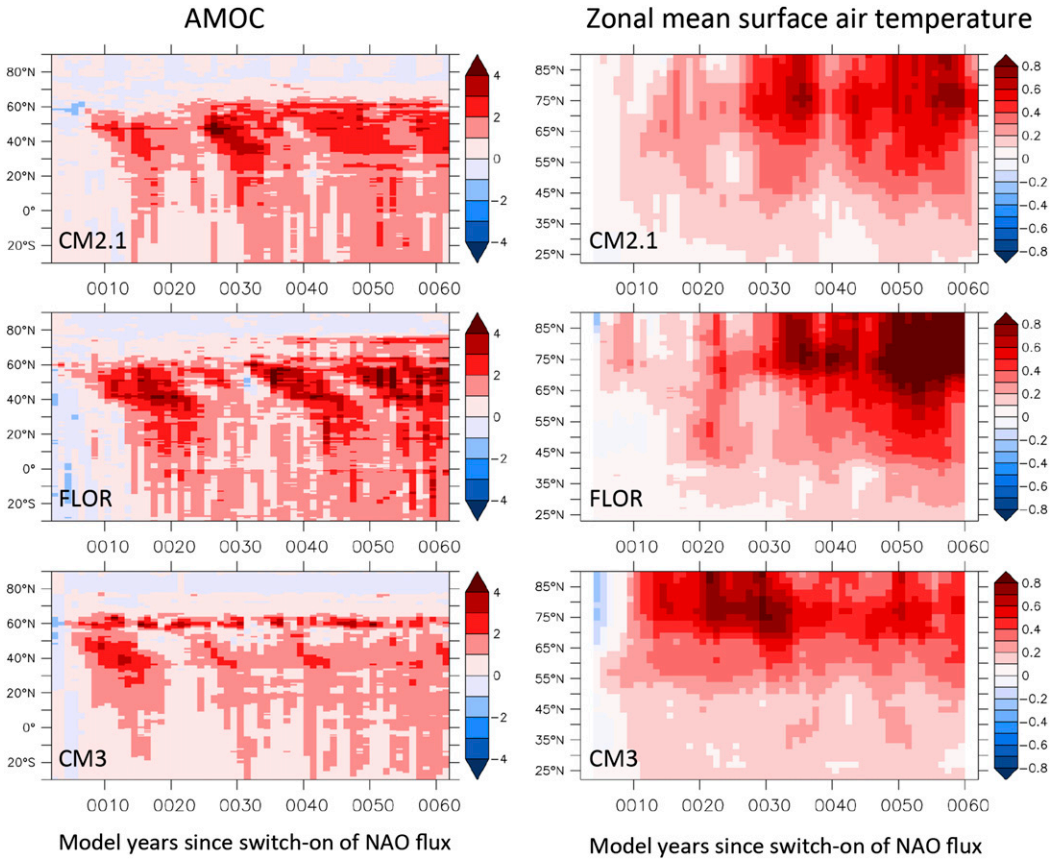

FIG. 14. Response of (left) AMOC (Sv) and (right) zonally averaged surface air temperature (K) to sudden switch on of NAO related heat flux forcing: (top) CM2.1, (middle) FLOR, and (bottom) CM3. Time is listed along the *x* axis in years and latitude is on the *y* axis.

scale of internal variability (approximately 15–20 yr for CM2.1 and longer for FLOR and CM3). The amplitude of the AMOC variations is largely independent of the time scale of forcing for time scales longer than 20 yr.

The response to NAO-like atmospheric forcing has previously been studied in ocean-only models (Visbeck et al. 1998; Eden and Willebrand 2001; Eden and Jung 2001; Lohmann et al. 2009; Zhai et al. 2014) and ocean reanalyses (Huang et al. 2012), and an approximate 5–10-yr time scale of the ocean's response to the NAO has also been shown. While past studies on this topic have primarily used ocean-only models, we have employed here a fully coupled ocean–atmosphere model to explore the impact of the simulated ocean changes back onto the rest of the climate system. This lagged response of the AMOC to variations of the NAO is important for interpreting the AMOC response to anthropogenic forcing (Delworth and Dixon 2000) and is an important physical underpinning for decadal prediction (Yeager et al. 2012; Yeager and Danabasoglu 2014; Hermanson et al. 2014).

The large-scale climatic response to NAO-induced AMOC variations is assessed as a function of time scale. While the amplitude of AMOC variations does not vary much as the time scale of forcing is increased from 20 to 100 yr, the amplitude of the large-scale climatic response increases substantially. At longer time scales the time integral of the ocean heat transport variations increases since the ocean heat transport is above (or below) normal for longer periods of time, leading to larger climatic impacts. These impacts include larger reductions (or increases) of sea ice and snow cover, which in turn increase (reduce) the impacts of albedo feedback, leading to further amplification. For example, the response of NH extratropical surface air temperature to NAO variations of the same amplitude is 3 times larger for the case of forcing at 100 years than at 20 years. This dependence may be a crucial factor in assessing the impact of NAO-induced AMOC variations on past climates. Similar amplification can be seen in the NAO-induced AMOC impacts on Artic sea ice and large-scale atmospheric circulation, including changes in tropical atmospheric circulation of relevance for tropical storms.

We perform identical experiments with three different models in order to test the robustness of the results. We find

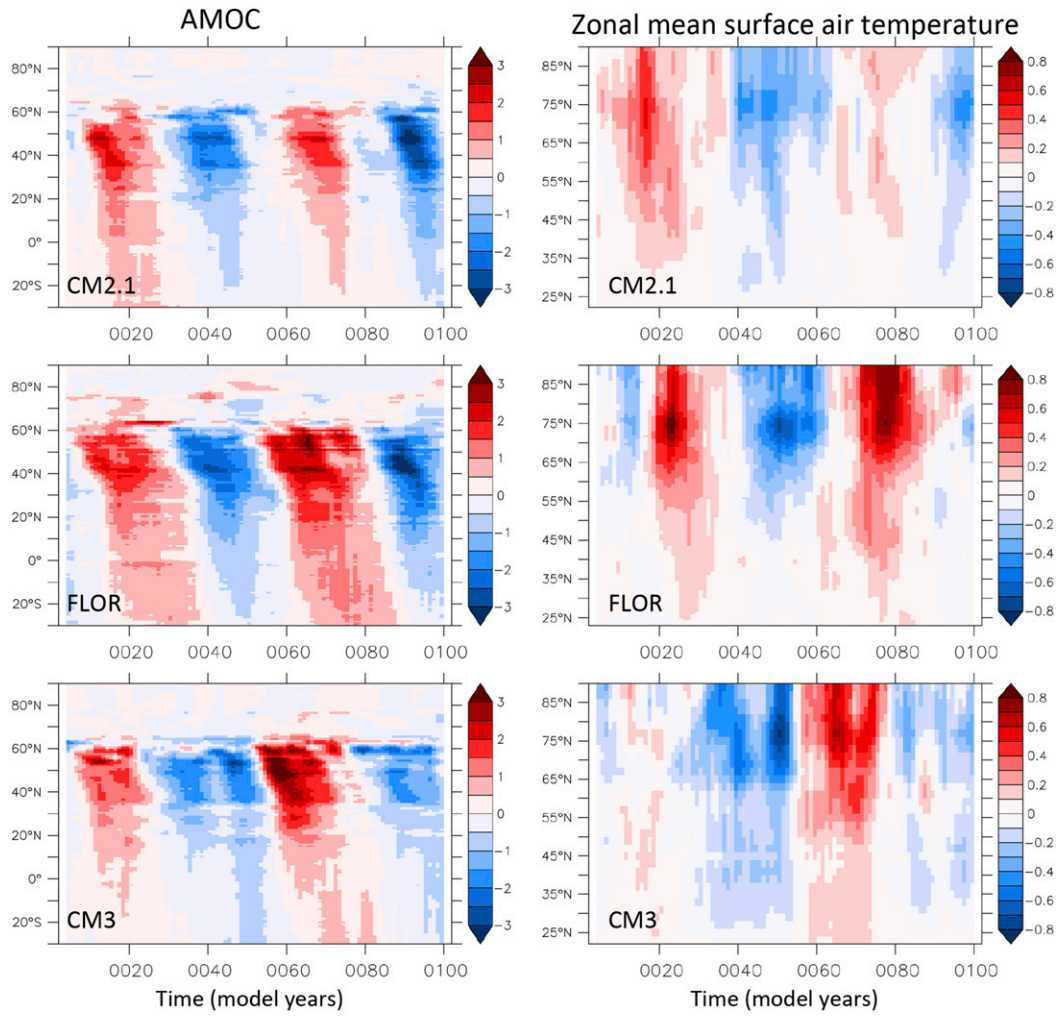

FIG. 15. Response of (left) AMOC (Sv) and (right) zonally averaged surface air temperature (K) to sinusoidal NAO heat flux forcing with amplitude of one standard deviation of the NAO time series and period of 50 yr: (top) CM2.1, (middle) FLOR, and (bottom) CM3. Time is listed along the *x* axis in years and latitude is on the *y* axis.

that the primary results are robust across the models, although details of the amplitudes of the response can vary.

These simulations focus on the response to NAO-induced surface heat flux anomalies. Preliminary experiments showed that heat flux forcing was the dominant term influencing AMOC variability at longer time scales in these models. However, it should be noted that these models all use a relatively coarse ocean model, with horizontal resolution of approximately 1°. The response of a model with much finer resolution and more energetic flows could be quite different, with a potentially larger sensitivity to momentum fluxes. This is especially relevant in light of the observed AMOC weakening associated with anomalous winds in 2009/10 (Roberts et al. 2013).

We speculate that the biases of the models used in this study will likely have some impact on their estimate of NAO-induced AMOC variability and its climatic impact (Menary et al. 2015). For example, the FLOR model has a tendency for excessive sea ice in portions of the North Atlantic and adjacent regions, especially in the Barents Sea. This could overestimate the impact of ice–albedo feedbacks. Similarly, the albedos associated with sea ice and snow cover on sea ice in CM2.1 are perhaps on the lower end of observational estimates, thereby potentially underestimating ice–albedo feedbacks in CM2.1. Simulated NH summer sea ice in CM2.1 is also less than observed (Delworth et al. 2006), potentially reducing ice–albedo feedbacks. In addition, other biases, such as the displacement of the Gulf Stream and the lack of intense boundary currents and frontal zones, could also have some impact on the overall estimates of variability and the sensitivity to NAO-induced AMOC variability. Recent work (Vecchi et al. 2014) has shown that reducing biases in the tropical Pacific is associated

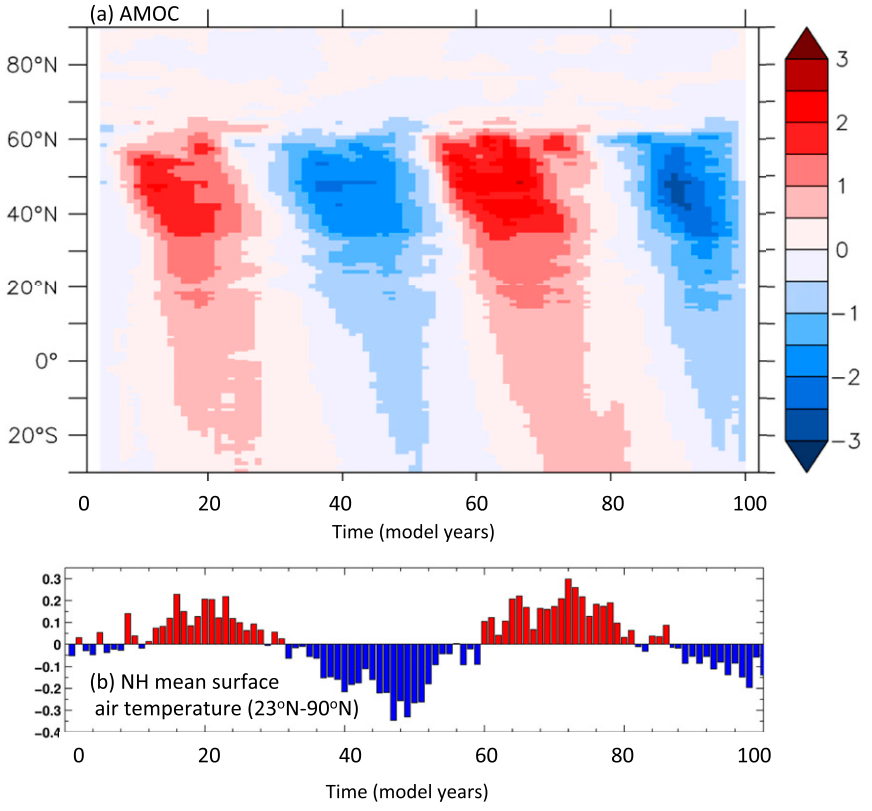

FIG. 16. Response to 50-yr NAO heat flux forcing calculated as the ensemble-mean response from CM2.1, FLOR, and CM3. We first calculate the ensemble mean using each model and then compute the mean of those three ensemble means. Time is listed in years along the x axis, indicating years since switching on the NAO-related heat fluxes. (a) AMOC response (Sv) as a function of latitude and time. (b) NH mean surface air temperature response (K) averaged over the domain 23°–90°N.

with an improved simulation of ENSO, providing support to the idea that reducing model biases could lead to improved simulation of variability.

The amplitude of the NAO forcing used in the present study is comparable to the interdecadal-scale variations observed in the NAO over the last century. The amplitude of the forcing used here corresponds to one standard deviation (a value of 1.9) of the NAO station index time series (NAO station data from https://climatedataguide.ucar.edu/climate-data/hurrell-north-atlantic-oscillation-nao-index-station-based). In the above observed NAO dataset, the NAO was greater than 2.0 in the early twentieth century, declined to less than −2.0 in the late 1960s, and increased to values greater than 2.0 in the 1990s. These observed interdecadal swings are comparable to the amplitude of the NAO index changes applied in this study. This suggests that variations of the NAO could have a significant impact on the AMOC and large-scale climate over the last century, including sea level in the western North Atlantic. For example, in our simulations a swing of the NAO corresponding to two standard deviations can alter NH extratropical surface air temperature by approximately 0.4 K. On sufficiently long time scales this swing would also lead to substantial changes in tropical Atlantic atmospheric circulation of relevance for tropical storm formation.

One interesting aspect is that the impact of AMOC fluctuations is dependent to some extent on albedo feedback. This suggests that as the climate system warms in response to increasing greenhouse gases and as Arctic sea ice and snow cover diminishes, the climatic impact of AMOC fluctuations would also be reduced. Conversely, in colder climates with more extensive sea ice, these effects could be larger.

An important aspect of the present study is that we have employed an idealized representation of the flux forcing associated with the NAO, treating the NAO as a static spatial pattern. In reality the spatial characteristics of the NAO vary over time (Hurrell and Deser 2009; Moore et al. 2013), and this could complicate the interpretation offered by our idealized framework.

The results of this study are of course limited by the fidelity of the models employed, particularly in terms of

the ocean component. The models are unable to resolve oceanic mesoscale eddies or the effects of deep overflows, such as over the sills between Greenland and Iceland or near the Faeroe banks. The model ocean itself has relatively large viscosity, resulting in weak boundary currents. In addition, the impacts of intense cyclones and their influence on air–sea interactions are missing. Nevertheless, it is likely that these models capture important relationships between the NAO, the AMOC, and larger-scale climate. These relationships are strongly influenced by oceanic adjustment to sustained changes in the NAO, involving changes in the AMOC and oceanic heat transport and their subsequent influence on the atmosphere, including radiative feedback processes.

Acknowledgments. We wish to thank Drs. Alistair Adcroft, Yohan Ruprich-Robert, and Liping Zhang for very helpful comments on an earlier version of this manuscript. We thank the editor and three anonymous reviewers for very valuable comments on preliminary versions of this manuscript.

REFERENCES

Biastoch, A., C. W. Böning, J. Getzlaff, J.-M. Molines, and G. Madec, 2008: Causes of interannual–decadal variability in the meridional overturning circulation of the midlatitude North Atlantic Ocean. *J. Climate*, **21**, 6599–6615, doi:10.1175/2008JCLI2404.1.

Bindoff, N. L., and Coauthors, 2013: Detection and attribution of climate change: From global to regional. *Climate Change 2013: The Physical Science Basis*, T. F. Stocker et al., Eds., Cambridge University Press, 867–952. [Available online at http://www.climatechange2013.org/images/report/WG1AR5_Chapter10_FINAL.pdf.]

Bjerknes, J., 1964: Atlantic air-sea interaction. *Advances in Geophysics*, Vol. 10, Academic Press, 1–82.

Chylek, P., C. K. Folland, G. Lesins, M. K. Dubey, and M. Wang, 2009: Arctic air temperature change amplification and the Atlantic multidecadal oscillation. *Geophys. Res. Lett.*, **36**, L14801, doi:10.1029/2009GL038777.

Cullen, H. M., A. Kaplan, P. A. Arkin, and P. B. deMenocal, 2002: Impact of the North Atlantic Oscillation on Middle Eastern climate and streamflow. *Climatic Change*, **55**, 315–338, doi:10.1023/A:1020518305517.

Danabasoglu, G., S. G. Yeager, Y.-O. Kwon, J. J. Tribbia, A. S. Phillips, and J. W. Hurrell, 2012: Variability of the Atlantic meridional overturning circulation in CCSM4. *J. Climate*, **25**, 5153–5172, doi:10.1175/JCLI-D-11-00463.1.

Dee, D. P., and Coauthors, 2011: The ERA-Interim reanalysis: Configuration and performance of the data assimilation system. *Quart. J. Roy. Meteor. Soc.*, **137**, 553–597, doi:10.1002/qj.828.

Delworth, T. L., and K. W. Dixon, 2000: Implications of the recent trend in the Arctic/North Atlantic Oscillation for the North Atlantic thermohaline circulation. *J. Climate*, **13**, 3721–3727, doi:10.1175/1520-0442(2000)013<3721:IOTRTI>2.0.CO;2.

——, and R. J. Greatbatch, 2000: Multidecadal thermohaline circulation variability driven by atmospheric surface flux forcing. *J. Climate*, **13**, 1481–1495, doi:10.1175/1520-0442(2000)013<1481:MTCVDB>2.0.CO;2.

——, and M. E. Mann, 2000: Observed and simulated multidecadal variability in the Northern Hemisphere. *Climate Dyn.*, **16**, 661–676, doi:10.1007/s003820000075.

——, S. Manabe, and R. J. Stouffer, 1993: Interdecadal variations of the thermohaline circulation in a coupled ocean–atmosphere model. *J. Climate*, **6**, 1993–2011, doi:10.1175/1520-0442(1993)006<1993:IVOTTC>2.0.CO;2.

——, and Coauthors, 2006: GFDL's CM2 global coupled climate models. Part I: Formulation and simulation characteristics. *J. Climate*, **19**, 643–674, doi:10.1175/JCLI3629.1.

Donner, L. J., and Coauthors, 2011: The dynamical core, physical parameterizations, and basic simulation characteristics of the atmospheric component AM3 of the GFDL global coupled model CM3. *J. Climate*, **24**, 3484–3519, doi:10.1175/2011JCLI3955.1.

Eden, C., and T. Jung, 2001: North Atlantic interdecadal variability: Oceanic response to the North Atlantic Oscillation (1865–1997). *J. Climate*, **14**, 676–691, doi:10.1175/1520-0442(2001)014<0676:NAIVOR>2.0.CO;2.

——, and J. Willebrand, 2001: Mechanism of interannual to decadal variability of the North Atlantic circulation. *J. Climate*, **14**, 2266–2280, doi:10.1175/1520-0442(2001)014<2266:MOITDV>2.0.CO;2.

Frankcombe, L. M., A. von der Heydt, and H. A. Dijkstra, 2010: North Atlantic multidecadal climate variability: An investigation of dominant time scales and processes. *J. Climate*, **23**, 3626–3638, doi:10.1175/2010JCLI3471.1.

Frankignoul, C., G. Gastineau, and Y.-O. Kwon, 2013: The influence of the AMOC variability on the atmosphere in CCSM3. *J. Climate*, **26**, 9774–9790, doi:10.1175/JCLI-D-12-00862.1.

Frierson, D. M. W., and Coauthors, 2013: Contribution of ocean overturning circulation to tropical rainfall peak in the Northern Hemisphere. *Nat. Geosci.*, **6**, 940–944, doi:10.1038/ngeo1987.

Gámiz-Fortis, S. R., D. Pozo-Vázquez, M. J. Esteban-Parra, and Y. Castro-Díez, 2002: Spectral characteristics and predictability of the NAO assessed through singular spectral analysis. *J. Geophys. Res.*, **107**, 4685, doi:10.1029/2001JD001436.

Gerber, E. P., and G. K. Vallis, 2009: On the zonal structure of the North Atlantic Oscillation and annular modes. *J. Atmos. Sci.*, **66**, 332–352, doi:10.1175/2008JAS2682.1.

Goddard, P. B., J. Yin, S. M. Griffies, and S. Zhang, 2015: An extreme event of sea-level rise along the Northeast coast of North America in 2009–2010. *Nat. Commun.*, **6**, 6346, doi:10.1038/ncomms7346.

Griffies, S. M., and Coauthors, 2011: The GFDL CM3 coupled climate model: Characteristics of the ocean and sea ice simulations. *J. Climate*, **24**, 3520–3544, doi:10.1175/2011JCLI3964.1.

Hermanson, L., R. Eade, N. H. Robinson, N. J. Dunstone, M. B. Andrews, J. R. Knight, A. A. Scaife, and D. M. Smith, 2014: Forecast cooling of the Atlantic subpolar gyre and associated impacts. *Geophys. Res. Lett.*, **41**, 5167–5174, doi:10.1002/2014GL060420.

Huang, B., Y. Xue, A. Kumar, and D. W. Behringer, 2012: AMOC variations in 1979–2008 simulated by NCEP operational ocean data assimilation system. *Climate Dyn.*, **38**, 513–525, doi:10.1007/s00382-011-1035-z.

Hurrell, J. W., 1995: Decadal trends in the North Atlantic Oscillation: Regional temperatures and precipitation. *Science*, **269**, 676–679, doi:10.1126/science.269.5224.676.

——, 1996: Influence of variations in extratropical wintertime teleconnections on Northern Hemisphere temperature. *Geophys. Res. Lett.*, **23**, 665–668, doi:10.1029/96GL00459.

——, and C. Deser, 2009: North Atlantic climate variability: The role of the North Atlantic Oscillation. *J. Mar. Syst.*, **78**, 28–41, doi:10.1016/j.jmarsys.2008.11.026.

Knight, J. R., R. Allan, C. K. Folland, M. Vellinga, and M. E. Mann, 2005: A signature of persistent natural thermohaline circulation cycles in observed climate. *Geophys. Res. Lett.*, **32**, L20708, doi:10.1029/2005GL024233.

Kuhlbrodt, T., A. Griesel, M. Montoya, A. Levermann, M. Hofmann, and S. Rahmstorf, 2007: On the driving processes of the Atlantic meridional overturning circulation. *Rev. Geophys.*, **45**, RG2001, doi:10.1029/2004RG000166.

Kwon, Y.-O., and C. Frankignoul, 2012: Stochastically-driven multidecadal variability of the Atlantic meridional overturning circulation in CCSM3. *Climate Dyn.*, **38**, 859–876, doi:10.1007/s00382-011-1040-2.

Li, J., C. Sun, and F.-F. Jin, 2013: NAO implicated as a predictor of Northern Hemisphere mean temperature multidecadal variability. *Geophys. Res. Lett.*, **40**, 5497–5502, doi:10.1002/2013GL057877.

Lohmann, K., H. Drange, and M. Bentsen, 2009: Response of the North Atlantic subpolar gyre to persistent North Atlantic oscillation like forcing. *Climate Dyn.*, **32**, 273–285, doi:10.1007/s00382-008-0467-6.

McCarthy, G. D., I. D. Haigh, J. J.-M. Hirschi, J. P. Grist, and D. A. Smeed, 2015: Ocean impact on decadal Atlantic climate variability revealed by sea-level observations. *Nature*, **521**, 508–510, doi:10.1038/nature14491.

Medhaug, I., H. R. Langehaug, T. Eldevik, T. Furevik, and M. Bentsen, 2012: Mechanisms for decadal scale variability in a simulated Atlantic meridional overturning circulation. *Climate Dyn.*, **39**, 77–93, doi:10.1007/s00382-011-1124-z.

Menary, M. B., W. Park, K. Lohmann, M. Vellinga, M. D. Palmer, M. Latif, and J. H. Jungclaus, 2012: A multimodel comparison of centennial Atlantic meridional overturning circulation variability. *Climate Dyn.*, **38**, 2377–2388, doi:10.1007/s00382-011-1172-4.

——, D. L. R. Hodson, J. I. Robson, R. T. Sutton, R. A. Wood, and J. A. Hunt, 2015: Exploring the impact of CMIP5 model biases on the simulation of North Atlantic decadal variability. *Geophys. Res. Lett.*, **42**, 5926–5934, doi:10.1002/2015GL064360.

Milly, P. C. D., and Coauthors, 2014: An enhanced model of land water and energy for global hydrologic and Earth-system studies. *J. Hydrometeor.*, **15**, 1739–1761, doi:10.1175/JHM-D-13-0162.1.

Moore, G. W. K., I. A. Renfrew, and R. S. Pickart, 2013: Multidecadal mobility of the North Atlantic Oscillation. *J. Climate*, **26**, 2453–2466, doi:10.1175/JCLI-D-12-00023.1.

Park, W., and M. Latif, 2008: Multidecadal and multicentennial variability of the meridional overturning circulation. *Geophys. Res. Lett.*, **35**, L22703, doi:10.1029/2008GL035779.

Roberts, C. D., and Coauthors, 2013: Atmosphere drives recent interannual variability of the Atlantic meridional overturning circulation at 26.5°N. *Geophys. Res. Lett.*, **40**, 5164–5170, doi:10.1002/grl.50930.

Scaife, A. A., C. K. Folland, L. V. Alexander, A. Moberg, and J. R. Knight, 2008: European climate extremes and the North Atlantic Oscillation. *J. Climate*, **21**, 72–83, doi:10.1175/2007JCLI1631.1.

Shaffrey, L., and R. Sutton, 2006: Bjerknes compensation and the decadal variability of the energy transports in a coupled climate model. *J. Climate*, **19**, 1167–1181, doi:10.1175/JCLI3652.1.

Steinman, B. A., M. E. Mann, and S. K. Miller, 2015: Atlantic and Pacific multidecadal oscillations and Northern Hemisphere temperatures. *Science*, **347**, 988–991, doi:10.1126/science.1257856.

Sutton, R. T., and D. Hodson, 2005: Atlantic Ocean forcing of North American and European summer climate. *Science*, **309**, 115–118, doi:10.1126/science.1109496.

——, and B. Dong, 2012: Atlantic Ocean influence on a shift in European climate in the 1990s. *Nat. Geosci.*, **5**, 788–792, doi:10.1038/ngeo1595.

Trigo, R. M., T. J. Osborn, and J. M. Corte-Real, 2002: The North Atlantic Oscillation influence on Europe: Climate impacts and associated physical mechanisms. *Climate Res.*, **20**, 9–17, doi:10.3354/cr020009.

Tulloch, R., and J. Marshall, 2012: Exploring mechanisms of variability and predictability of Atlantic meridional overturning circulation in two coupled climate models. *J. Climate*, **25**, 4067–4080, doi:10.1175/JCLI-D-11-00460.1.

Vecchi, G. A., and Coauthors, 2014: On the seasonal forecasting of regional tropical cyclone activity. *J. Climate*, **27**, 7994–8016, doi:10.1175/JCLI-D-14-00158.1.

Vellinga, M., and P. Wu, 2004: Low-latitude freshwater influence on centennial variability of the Atlantic thermohaline circulation. *J. Climate*, **17**, 4498–4511, doi:10.1175/3219.1.

Visbeck, M., H. Cullen, G. Krahmann, and N. Naik, 1998: An ocean model's response to North Atlantic Oscillation-like wind forcing. *Geophys. Res. Lett.*, **25**, 4521–4524, doi:10.1029/1998GL900162.

Wunsch, C., 1999: The interpretation of short climate records, with comments on the North Atlantic and Southern Oscillations. *Bull. Amer. Meteor. Soc.*, **80**, 245–255, doi:10.1175/1520-0477(1999)080<0245:TIOSCR>2.0.CO;2.

Yang, H., Y. Wang, and Z. Liu, 2013: A modelling study of the Bjerknes compensation in the meridional heat transport in a freshening ocean. *Tellus*, **65A**, 18480, doi:10.3402/tellusa.v65i0.18480.

Yeager, S., and G. Danabasoglu, 2012: Sensitivity of Atlantic meridional overturning circulation variability to parameterized Nordic sea overflows in CCSM4. *J. Climate*, **25**, 2077–2103, doi:10.1175/JCLI-D-11-00149.1.

——, and ——, 2014: The origins of late-twentieth-century variations in the large-scale North Atlantic circulation. *J. Climate*, **27**, 3222–3247, doi:10.1175/JCLI-D-13-00125.1.

——, A. Karspeck, G. Danabasoglu, J. Tribbia, and H. Teng, 2012: A decadal prediction case study: Late twentieth-century North Atlantic Ocean heat content. *J. Climate*, **25**, 5173–5189, doi:10.1175/JCLI-D-11-00595.1.

Zhai, X., H. L. Johnson, and D. P. Marshall, 2014: A simple model of the response of the Atlantic to the North Atlantic Oscillation. *J. Climate*, **27**, 4052–4069, doi:10.1175/JCLI-D-13-00330.1.

Zhang, R., and T. L. Delworth, 2005: Simulated tropical response to a substantial weakening of the Atlantic thermohaline circulation. *J. Climate*, **18**, 1853–1860, doi:10.1175/JCLI3460.1.

——, and G. K. Vallis, 2007: The role of bottom vortex stretching on the path of the North Atlantic western boundary current and on the northern recirculation gyre. *J. Phys. Oceanogr.*, **37**, 2053–2080, doi:10.1175/JPO3102.1.

——, T. L. Delworth, and I. M. Held, 2007: Can the Atlantic Ocean drive the observed multidecadal variability in Northern Hemisphere mean temperature? *Geophys. Res. Lett.*, **34**, L02709, doi:10.1029/2006GL028683.

Zhu, X., and J. Jungclaus, 2008: Interdecadal variability of the meridional overturning circulation as an ocean internal mode. *Climate Dyn.*, **31**, 731–741, doi:10.1007/s00382-008-0383-9.